

DynaQuant: Compressing Deep Learning Training Checkpoints via Dynamic Quantization

Amey Agrawal¹, Sameer Reddy¹, Satwik Bhattamishra², Venkata Prabhakara Sarath Nookala¹,
Vidushi Vashishth¹, Kexin Rong¹, Alexey Tumanov¹

¹Georgia Institute of Technology, ²University of Oxford

{ameyagrawal,sreddy65,vnookala3,vvashishth3,krong,atumanov}@gatech.edu,satwik.bmishra@cs.ox.ac.uk

ABSTRACT

With the increase in the scale of Deep Learning (DL) training workloads in terms of compute resources and time consumption, the likelihood of encountering in-training failures rises substantially, leading to lost work and resource wastage. Such failures are typically offset by a checkpointing mechanism, which comes at the cost of storage and network bandwidth overhead. State-of-the-art approaches involve lossy model compression mechanisms, which induce a tradeoff between the resulting model quality (accuracy) and compression ratio. Delta compression is then used to further reduce the overhead by only storing the difference between consecutive checkpoints. We make a key enabling observation that the sensitivity of model weights to compression varies during training, and different weights benefit from different quantization levels (ranging from retaining full precision to pruning). We propose (1) a *non-uniform* quantization scheme that leverages this variation, (2) an efficient search mechanism that dynamically finds the best quantization configurations, and (3) a quantization-aware delta compression mechanism that rearranges weights to minimize checkpoint differences, thereby maximizing compression.

We instantiate these contributions in DynaQuant—a framework for DL workload checkpoint compression. Our experiments show that DynaQuant consistently achieves a better tradeoff between accuracy and compression ratios compared to prior works, enabling a compression ratio up to 39x and withstanding up to 10 restores with negligible accuracy impact for fault-tolerant training. DynaQuant achieves at least an order of magnitude reduction in checkpoint storage overhead for training failure recovery as well as transfer learning use cases without any loss of accuracy.

1 INTRODUCTION

Large-scale Deep Learning (DL) training workloads, increasingly require weeks or months of compute time on clusters with hundreds of GPUs [88]. The expanding scale of resource requirements coupled with longer training duration leads to a higher probability of failure at some point during the run. Distributed training systems conventionally resort to the most recent checkpoint to recover from failures. Frequent checkpointing is necessary to minimize work wasted due to failures, but it comes at the cost of increased storage and network bandwidth overhead, particularly in multi-tenant environments. For instance, a single checkpoint for a 175B GPT-3 [10] model is 2.3 TB. This tradeoff between the cost of frequent checkpoints and the cost of work lost due to failures highlights the need for an effective compression mechanism to minimize checkpointing overhead. The large size of model checkpoints also impedes the efficacy of operational aspects of deep-learning systems. The

checkpoint size not only introduces storage complications but also becomes a logistical hurdle in remote transfers, deployment, auditing, and debugging activities.

To confront the challenges presented by large model checkpoint sizes, several works have explored various compression techniques [13, 27, 47, 52]. These systems typically deploy a dual-phase compression strategy. In the initial phase, lossy compression is applied through a technique called quantization, which essentially maps a larger set of values to a smaller set, thereby reducing the data footprint. The remarkable aspect of using quantization lies in its compatibility with the error-resilient nature of deep learning models, allowing for reduced storage requirements without a significant sacrifice in accuracy. Subsequently, lossless delta encoding techniques [13, 27, 47, 52] are employed to record merely the differences between successive checkpoints, further enhancing compression efficiency.

However, the existing model compression frameworks face shortcomings either in terms of suboptimal compression or lead to undesirable accuracy degradation—issues most pronounced in large-scale models where efficient compression is most needed. This occurs for two fundamental reasons. First, model parameters exhibit different levels of sensitivity to compression. Systems such as Check-N-Run [27] and QD-Compressor [52] adopt uniform quantization strategies that provide all parameters with the same level of resolution – oblivious to the level of their impact on the model quality. Secondly, it’s observed that models, as they accrue knowledge over the course of training, exhibit increasing susceptibility to the limitations imposed by quantization. Yet, prevailing compression systems adhere to fixed quantization configurations, like a preset number of quantization bins, throughout the training lifecycle.

To overcome these limitations, we present DynaQuant—an efficient, transparent in-training model checkpoint compression system for DL workloads (Figure 1). DynaQuant is premised on the observation that not all model parameters contribute equally to model quality, and this contribution varies as the model trains. This observation informs three main aspects of DynaQuant.

First, DynaQuant provides a comprehensive quantization configuration space that partitions model parameters into three groups based on their significance: parameters preserved with full precision (unchanged), pruned parameters (set to zero), and quantized parameters. For the quantized parameters, DynaQuant proposes a novel *non-uniform* quantization approach using a sketch-based approximate K-Means clustering algorithm. This approach enables more

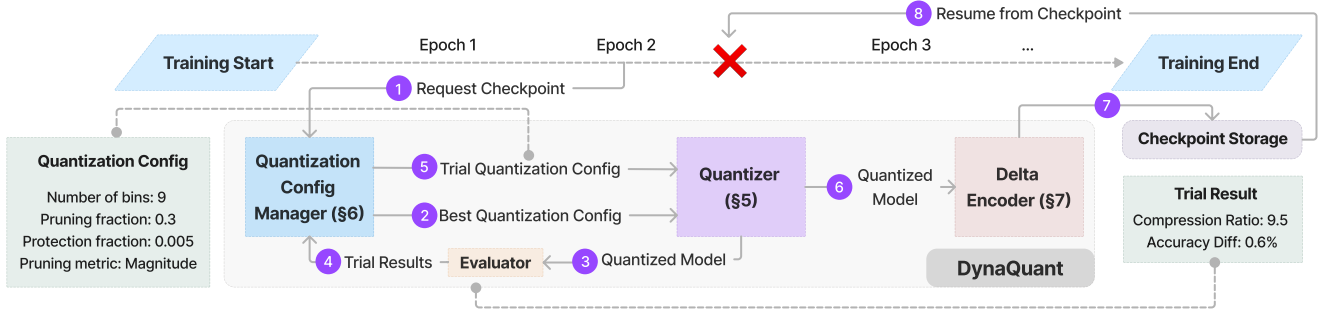


Figure 1: High-level workflow of a checkpoint compression and saving request, and resumption of training on failure from a saved compressed checkpoint in DynaQuant.

effective compression by reducing the number of required quantization bins¹ by 2-3× compared to uniform quantization while introducing minimal runtime overhead. We show that our clustering approach is up to 65× faster than naive K-means clustering-based quantization.

Second, DynaQuant includes an efficient dynamic quantization configuration search component. This component automatically adapts the quantization configuration as parameters’ sensitivity towards compression changes over training time. This has the combined benefit of improving compression performance and alleviating the cognitive burden on ML practitioners to manually choose these configurations.

Finally, DynaQuant implements a novel quantization-aware delta encoding scheme, which leverages our insight that most parameters remain in the same quantization bin across consecutive checkpoints. Our delta encoding scheme rearranges the model parameters such that parameters for each quantization bucket are stored separately, improving delta encoding efficiency with compression ratios 3-4× higher than existing delta compression schemes.

DynaQuant builds on the following principal contributions:

- A novel *non-uniform* quantization approach using approximate K-Means clustering. This helps achieve high-quality quantized models with minimal runtime overhead. We show that our quantization scheme achieves consistent performance on a variety of DL model architectures while requiring 2-3× fewer quantization bins compared to uniform quantization approaches enabling more efficient compression.
- A mechanism for efficient, automatic quantization configuration search space navigation during training.
- A delta compression algorithm with effective run length encoding [36] enabled by quantization-aware model parameter rearrangement.

We evaluate DynaQuant’s end-to-end performance for fault-tolerant training on a variety of popular DL models including convolution neural networks (CNNs) (ResNet 152 [44]), language transformers (BERT Base [22], GPT-2 Medium [73] & Pythia 1b [9]), and vision transformers (ViT L32 [26]), with the training cost exceeding 650 GPU hours for the largest models (GPT-2 Medium and ViT L32)

¹In contrast to previous works on quantization, which typically restrict the number of quantization bins to powers of two for computational efficiency, our approach allows for the use of any arbitrary number of quantization bins. This flexibility enables us to achieve improved compression performance.

on NVIDIA A40 GPUs. DynaQuant reduces checkpoint storage requirement by 26-39× for fault-tolerant training and sustains up to ten failures (reasonable for multi-day training jobs) with negligible impact on the accuracy of the trained model, achieving a 1.3-3.3× improvement over state-of-the-art methods. DynaQuant can also be utilized to reduce the storage overhead of snapshots of pre-trained models used for transfer learning by 10× with no impact on the performance of the fine-tuned model at all. Overall, DynaQuant can achieve at least an order of magnitude checkpoint overhead reduction on both use cases with minimal loss of accuracy.

2 BACKGROUND AND USE CASES

We start by introducing the notion of checkpointing in deep learning systems and highlight a variety of scenarios where model checkpoint compression is beneficial. Model checkpoints serve as snapshots of a deep learning model at a certain stage in its training process. They encompass the model’s architecture, learned parameters, and optimizer state. One can think of checkpoints as analogous to code commits in version control systems, where each checkpoint represents a version of the model at a specific stage of its development. In the rest of this section, we describe several use cases for model checkpoint compression.

Failure Recovery In Training Workloads. Large-scale deep-learning training workloads are highly susceptible to various hardware and software failures. Any failure during this period prompts a recovery from the most recent checkpoint. Joen et al. [51] show that on average DL training workloads in a Microsoft cluster encounter a failure every 45 minutes (excluding early failures) due to various system and user errors. Zhang et al. [88] also observe that the training of the OPT-2 model required 100+ restarts due to failures across the span of two months. As we move toward developing not only larger but also more complex models and distributed training systems, the likelihood of experiencing system failures is expected to rise. Simultaneously, constraints on bandwidth and storage capacity, especially in shared multi-tenant environments, limit the frequency of checkpoints. This creates tension between frequent checkpointing to minimize wasted work and managing the storage and network checkpointing overheads. Addressing this challenge calls for a compression mechanism that enables more frequent checkpoints with minimal overhead.

	CNR [27]	QD [52]	LC [13]	DDNN [47]	GOBO [87]	DynaQuant
In-training	✓	✓	✓	✓	✗	✓
Low Overhead	✓	✓	✓	✓	✗	✓
Model Agnostic	✗	✓	✓	✓	✓	✓
Scalable	✓	✓	✓	✓	✗	✓
Algorithmically Transparent	✓	✗	✓	✓	✓	✓
Dynamic Configuration Management	✗	✗	✗	✓	✗	✓
Non-uniform Quantization	✗	✗	✓	✗	✗	✓
Quantization-aware Delta Encoding	✗	✓	✓	✓	✗	✓

Table 1: Checkpoint compression systems: feature comparison.

Iterative Model Development. In the development of deep learning models, checkpoints are useful for multiple use cases including version control and continual learning. DL model development is an iterative process with bug fixes, hyperparameter tuning, and architectural adjustments. Given the substantial GPU hours invested in training, it is wasteful to discard progress just to make these adjustments. As a result, practitioners make these changes mid-way through training and resume the training from a stable checkpoint [1]. This prompts the need for an effective git-like version control system for models, to manage their development cycle. Beyond the training phase, production environments often require continuous updates to models in order to accommodate new data and maintain performance. In such scenarios, model checkpoints are preserved for extended periods for reasons such as debugging, reliability, and provenance. Delta-encoded checkpoints, where only the changes between successive checkpoints are stored, can help minimize storage requirements and streamline recovery processes in these use cases.

Model Hubs & Transfer Learning. Model hubs, such as Hugging Face [3], provide pre-trained models for a variety of tasks. These pre-trained models can be used for transfer learning, a process in which a pre-trained model is fine-tuned for a new task or domain. With the growth of the number of models on such hubs, the bandwidth required to transfer model checkpoints becomes a significant concern. For example, the BERT Base [22] model alone was downloaded more than 41 million times from the HuggingFace model hub [2] in a 30-day window as of August 2023. Model checkpoint compression can reduce the bandwidth required for transferring models between users and model hubs.

3 OVERVIEW

We propose DynaQuant to address the challenges associated with model checkpoint compression. In this section, we outline the design goals and ideas that underpin our solution and present an overview of key components in DynaQuant. Table 1 provides a high-level comparison with existing checkpoint compression systems and we provide a detailed discussion in Section 10.

3.1 Design Goals

DynaQuant aims to preserve model accuracy, even with multiple restores from compressed checkpoints, and to achieve this with

minimal storage overhead. Further, DynaQuant incorporates the following design objectives:

- **Low Overhead:** an optimized compression pipeline to ensure swift checkpointing, imposing no more than 0.5% overhead on training runtime.
- **Model Agnostic:** the quantization algorithm should be able to deal with a diverse set of model architectures including Convolutional Neural Networks, Transformer-based language models, and Vision Transformers, without requiring model-specific adjustments.
- **Scalable:** the ability to handle models with hundreds of millions to billions of parameters, circumventing slowdowns, and memory bottlenecks.
- **Algorithmically Transparent:** an absence of any interference with the original training algorithm, in contrast to quantization-aware training methods.

3.2 System Overview

Checkpoint requests in DynaQuant are processed in three stages as illustrated in Figure 1. First, **QUANTIZATION CONFIGURATION MANAGER** performs a distributed configuration search to identify a suitable quantization configuration (steps 2-5). Second, the model is compressed by **QUANTIZER** using the identified configuration (step 6). Third, the checkpoint is copied to CPU memory, where it is processed by the **DELTA ENCODER** (step 7).

This section provides a high-level overview on the three core components of DynaQuant: 1) **QUANTIZATION CONFIGURATION MANAGER**’s dynamic configuration management, 2) **QUANTIZER**’s non-uniform quantization, and 3) **DELTA ENCODER**’s quantization-aware delta encoding, each contributing to our design goals.

QUANTIZATION CONFIGURATION MANAGER. Most existing model checkpoint compression systems require users to specify the quantization configuration (i.e., number of quantization bins, pruning fraction, etc.) at the start of training. However, different models exhibit different sensitivity to compression, which also changes over time. Thus, statically determined quantization configuration results in inconsistent performance. Instead, DynaQuant’s **QUANTIZATION CONFIGURATION MANAGER** *dynamically* updates the quantization configuration throughout the training process.

To control the quality of quantized models, **QUANTIZATION CONFIGURATION MANAGER** allows the user to specify a threshold for maximum acceptable quality degradation during the checkpointing operation. The quality degradation is measured by evaluating the quantized model on a user-specified metric (typically change in accuracy or loss) using a small subset of data samples. Note that as long as the quantization error is small, the model quickly recovers to its original level of performance once the training is resumed.

Our quantization algorithm exposes a large configuration space that enables us to tailor-fit the quantization process for various models and quality requirements. However, a naive approach to navigating this large search space to find the optimal configuration can be prohibitively expensive. We leverage two key insights to optimize the configuration search: focusing on configurations similar to the best configuration in the previous round of checkpointing

and parallelizing the exploration of multiple candidate configurations in distributed training settings. We describe the configuration search at depth in Section 5.

QUANTIZER. The key enabler for DynaQuant’s consistent compression performance is our fast, *non-uniform* quantization scheme. We propose an approximate K-Means clustering-based quantization approach that provides high-quality quantized models while cutting runtime overhead by several orders of magnitude compared to other non-uniform quantization approaches. We design the quantization process to be fully model-agnostic to maintain the system’s versatility and adaptability across various models. Additionally, the QUANTIZER performs parameter pruning, which further reduces the size of the checkpoint by eliminating parameters that contribute to model performance the least. We elaborate on our quantization approach in Section 4.

DELTA ENCODER. Following the quantization phase, we perform lossless compression using a *quantization-aware* delta compression, which exploits the similarity between consecutive checkpoints. The DELTA ENCODER leverages a novel quantization-aware parameter rearrangement technique that enables efficient run-length encoding to reduce storage overhead by up to two orders of magnitude. We describe our delta compression process in Section 6.

4 QUANTIZER: FAST NON-UNIFORM QUANTIZATION AND PRUNING

This section outlines the design and implementation of the QUANTIZER. In DynaQuant, we perform quantization as a two-step operation. First, we partition parameters into three discreet groups. The least important parameters are pruned out, while a small set of most sensitive parameters are protected in high precision (bfloat16). The remaining intermediate parameters are quantized using our approximate K-Means clustering-based non-uniform quantization approach. The QUANTIZER compresses model weights given the fraction of weights to protect and prune along with the number of quantization bins (K-Means clusters) for remaining parameters.

In Section 4.1, we introduce the two metrics—magnitude and sensitivity—that Quantizer employs to ascertain the relative importance of each model parameter.

Section 4.2 is dedicated to elaborating the parameter partitioning algorithm to identify parameters for pruning or protection. We also present an approach that reduces the computational overhead of this operation through the use of mergeable quantile sketches.

Lastly, in Section 4.3, we introduce our approximate K-Means clustering algorithm and its application in non-uniform quantization. An overview of QUANTIZER’s workflow is shown in Figure 2.

4.1 Metrics for Parameter Ranking

First, we need to rank parameters by importance in order to assign them for protection, pruning, or quantization. The two popular metrics used to determine the importance of parameters are magnitude and sensitivity. As the name suggests, magnitude-based ranking approaches simply use the parameter magnitude as an importance score [32, 34, 40, 91]. The magnitude score $I_m(w)$ for parameter w is defined as $I_m(w) = |w|$. On the other hand, sensitivity-based ranking approaches attempt to estimate the impact on the end-to-end

loss value when a parameter is altered [24, 42, 57, 59, 67]. In the context of this paper, we use the first-order Taylor series approximation formulation of sensitivity for the sake of computational efficiency. The sensitivity score is defined as $I_s(w) = |\nabla \mathcal{L}(w)w|$, where \mathcal{L} represents the loss function and $\nabla \mathcal{L}(w)$ is the gradient of weight w with respect to the loss function.

It has been shown that magnitude-based parameter ranking approaches perform poorly in the early stage of training [77]. On the other hand, as we approach convergence, the first-order gradient values start to diminish, making the sensitivity metric less reliable. Some previous works [24, 42, 86] address this challenge by using second-order derivatives (Hessian), however, that adds significant computational overhead. As an alternative, we use a combination of sensitivity and magnitude to get a reliable ranking throughout the training process.

Figure 3b shows the distribution of parameters across the two ranking dimensions for a ResNet152 model trained on Imagenet data. While there is a strong correlation between magnitude and sensitivity, we observe a significant number of outliers, which have a high magnitude score but a low sensitivity score or vice versa. By ranking parameters across both the metrics, DynaQuant can identify and preserve these parameters.

Efficient Sensitivity Computation. To save computational resources, we reuse gradients computed during the training process for sensitivity estimates instead of calculating them separately. To avoid any GPU memory overhead, we asynchronously copy the gradients to pinned CPU memory as soon as the backward pass is completed. The gradient copy operation is overlapped with the optimizer step, data loading, and forward pass of the next batch, making the overhead of this operation negligible as shown in Figure 4. The copied gradient values are accumulated on the CPU using an exponential moving average $\text{EMA}_{g_w}^t = \beta * g_w^t + (1 - \beta) * \text{EMA}_{g_w}^{t-1}$, where $\text{EMA}_{g_w}^t$ is the exponential moving average of the gradient g_w at timestep t . We set the value of β to be 0.9 in all our experiments to emphasize the recent gradients. The gradient copy mechanism is only invoked for a limited preconfigured number of batches before checkpointing is scheduled to be performed to further avoid any impact on steady-state throughput. We identify that typically recording gradients for fifty batches is sufficient to get good sensitivity estimates.

4.2 Parameter Partitioning

Given the magnitude and sensitivity score for each model parameter, the QUANTIZER partitions the parameters into one of the three groups (Figure 3a).

Protection. DynaQuant preserves the most important model parameters in the high precision bfloat16 [54] format. Recent quantization studies [18, 21] show a significant reduction in quantization error when a few important weights are protected. This is consistent with the Lottery Ticket Hypothesis [32], which suggests that training a small fraction of high-importance weights in isolation can achieve performance similar to the full network.

Our experiments suggest that protecting a small fraction of both the highest magnitude and sensitivity parameters provides the best performance. We have recognized that protecting 0.05-0.1% weights

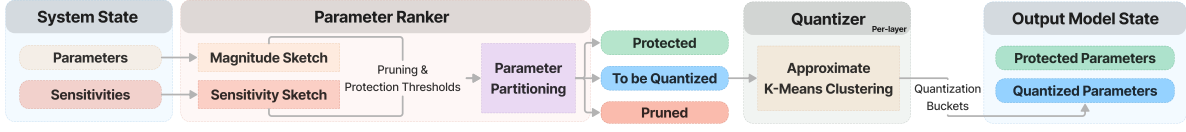
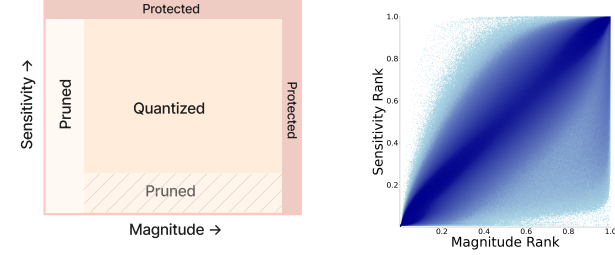


Figure 2: A high-level illustration of the quantization process in DynaQuant.



(a) Parameter partitioning schema in DynaQuant. (b) Parameter distribution for ResNet152 trained on Imagenet.

Figure 3: Model parameters are partitioned into three groups for pruning, protection, and quantization according to their magnitude and sensitivity scores.

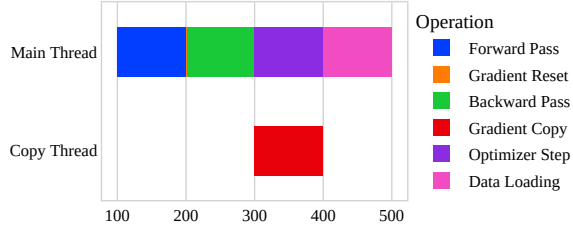


Figure 4: Schematic representation of asynchronous gradient offloading for efficient sensitivity computation in DynaQuant.

is sufficient in most conditions. In our experiments, the precise protection fraction is determined dynamically by the `QUANTIZATION CONFIGURATION MANAGER`. Based on the fraction (F_{prot}) of parameters to be protected, we identify the minimum magnitude (τ_{prot}^m) and sensitivity (τ_{prot}^s) thresholds for a parameter to qualify for protection. Given quantile function Q , we define protected parameters as,

$$\tau_{\text{prot}}^m = Q(|\Theta|, \frac{F_{\text{prot}}}{2}), \tau_{\text{prot}}^s = Q(\text{Sensitivity}(\Theta), \frac{F_{\text{prot}}}{2})$$

$$\Theta_{\text{prot}} = \{\theta \mid |\theta| > \tau_{\text{prot}}^m\} \cup \{\theta \mid \text{Sensitivity}(\theta) > \tau_{\text{prot}}^s\}$$

Pruning. We prune the least significant model parameters, based on the pruning fraction F_{prun} (typically between 10-40%) and pruning metric, (magnitude or sensitivity). An important consideration in the design of the pruning algorithm is the granularity level at which the pruning is performed. Layer-level pruning can degrade model quality due to different redundancy levels across the network layers. Conversely, global pruning may disproportionately affect different layer types (e.g., Convolution, Attention, Linear) in deep learning models due to varied weight distributions. To tackle this, we perform pruning on a *per-layer type* basis, using the same

pruning fraction across all layer types. We observed that in GPT-2 Medium, we can eliminate up to 30% parameters with a minimal effect on the model’s quality.

$$\tau_{\text{prun}} = Q(\text{PrunMetric}(\Theta), F_{\text{prun}}), \Theta_{\text{prun}} = \{\theta \mid \text{PrunMetric}(\theta) < \tau_{\text{prun}}\}$$

Efficient Parameter Partitioning via Quantile Sketches. Computing quantiles required for determining pruning and protection thresholds can be costly, especially for large models due to the log-linear time complexity of the operation. Moreover, in cases where models are trained via model parallelism, and parameters are distributed across different worker groups, computing global quantiles can be quite challenging.

To facilitate efficient partitioning of model parameters, we use a sketch-based quantile estimation algorithm that is a simplified and parallelized version of DDSketch [64]. This enables us to compute approximate quantile estimates in linear time with a configurable α -relative-error bound, that is, the sketch produces an estimated quantile value corresponding to the quantile value x_q such that $|\tilde{x}_q - x_q| \leq \alpha x_q$. For computing protection and pruning thresholds, that require tail quantiles, DDSketch’s relative error bounds outperform alternative quantile sketches that guarantee rank error. Furthermore, the quantile sketches are mergeable, which simplifies the computation of global quantile estimates from individual model shards.

The sketching algorithm transforms the input values into a logarithmic space and then divides them into an equal-width histogram (Figure 5). Due to the use of a logarithmic scale, we achieve varying levels of detail for different ranges of the original values. Specifically, smaller original values will land in narrower bins, while larger values will fall into broader bins. This allows the sketch to provide the α -relative error property of the sketch. To produce quantile estimates, the sketch sums up the buckets until it finds the bucket containing the desired quantile value.

The algorithm is outlined in Appendix A.1. We forgo the bucket merging step in the original DDSketch for ease of parallelization. This has limited impact in practice, as we observe that the number of buckets does not exceed a few thousand even for models with hundreds of millions of parameters with a strict relative error bound of 1%. We implement a highly parallelized version of this algorithm using Pytorch that can run on GPUs. We observe a 3-4 \times speed-up compared to off-the-shelf GPU-enabled implementation provided by CuPy [70] while using significantly less memory.

4.3 Non-uniform Quantization via Approximate K-Means

The remaining model parameters that are not pruned or protected go through quantization. Quantization reduces the precision of model parameters to lower-bit representations (e.g., from 32-bit

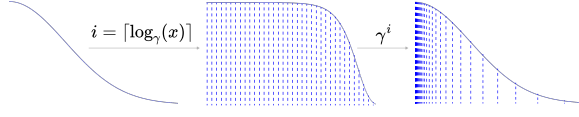


Figure 5: DDSketch’s log space transformation creates a histogram with value-dependent bucket width.

floating-point to 8-bit integers), leveraging redundancy and noise tolerance in large networks. Uniform quantization strategies create equally spaced quantization levels across the parameter space [16, 50, 85], while non-uniform quantization approaches use varying intervals between levels to adapt to the parameter distribution [12, 31, 65].

Non-uniform quantization techniques, such as via K-Means clustering [27, 39, 87], generally provide better compression and model quality. However, they have seen limited adoption in checkpoint compression systems due to their computational complexity. For instance, GOBO [87], utilizing a variant of K-Means clustering, takes roughly 50 minutes to quantize a relatively small model like ResNet-18 [44] (11.7 million parameters).

Algorithm 1: Approximate K-Means Clustering

Require: X {Input data points}
Require: α {Relative error bound}
Require: σ {Linear combination factor}
Require: k {Number of clusters}

- 1: $X_q, C_q \leftarrow \text{GetQuantileSketchHistogram}(X, \alpha)$ {Obtain log sketch histogram Algorithm 2 for coarse grain clustering. X_q are the histogram bucket centers and C_q are the corresponding frequencies.}
- 2: $\hat{X}_q, \hat{C}_q \leftarrow \text{Normalize}(X_q), \text{Normalize}(C_q)$
- 3: $W = \sigma * \hat{C}_q + (1 - \sigma) * |\hat{X}_q|$ {Compute sample weight for histogram buckets according to frequency and magnitude}
- 4: $\text{centers} \leftarrow \text{WeightedKMeans}(X_q, W, k)$ {Perform weighted k-means++ clustering on histogram keys and values}
- 5: **return** centers

4.3.1 Approximate K-Means Clustering. We introduce an efficient non-uniform quantization method leveraging approximate K-means clustering, which strikes a balance between high quantization quality and computational efficiency. Our key insight is to perform K-means clustering on histogram buckets of the parameters, rather than on the raw parameters themselves. This significantly reduces the computational burden of K-means clustering, resulting in up to $65\times$ speedup compared to the standard implementation in CuML [75] (refer to Section 9.3).

The two-step quantization algorithm is depicted in Figure 6. First, we group model parameters into coarse-grain buckets, utilizing the same log-space projection approach used for creating the quantile sketch in Section 4.2. We then perform weighted k-means clustering, where the histogram bins serve as the data and their heights as sample weights, to establish quantization boundaries. Two key optimizations enhance this clustering performance:

First, we introduce an additional parameter, σ , to our weighted K-Means to help balance the allocation of resolution between high-importance parameters with low frequency and high-frequency

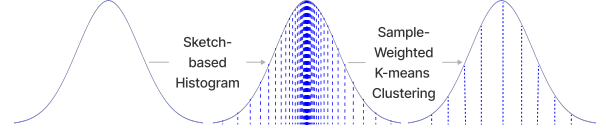


Figure 6: Two-step quantization: (1) group model parameters into coarse-grained buckets with sketch-based histogram computation. (2) cluster buckets using a sample weighted K-means clustering.

parameters with low importance. Usually, non-uniform clustering offers increased resolution to denser parameter spaces. However, this can lead to issues for neural network parameters, which typically follow a bell-curve distribution. Such a scheme would allocate greater resolution to values near zero—the peak of the bell—resulting in higher error for larger magnitude weights that tend to be more crucial for model performance. To address this, we calculate the sample weight of a bucket, b^i , as a linear combination of the bucket’s normalized frequency and magnitude: $w^i = \sigma * b_{\text{freq}}^i + (1 - \sigma) * b_{\text{mag}}^i$ (see line 2 in Algorithm 1). Our observations suggest that values of σ in the range 0.1 – 0.4 generally provide the best compression results. We fix the value of σ to 0.2 for all our experiments.

Second, the success of the K-Means clustering algorithm relies heavily on proper initialization. Inappropriate initialization can lead to suboptimal solutions and slower convergence. K-means++ [6] addresses this by ensuring the initial centroids are uniformly distributed across the space, often leading to near-optimal solutions with a single round of clustering. We enhance K-means++ to support sample-weighted clustering, with a detailed explanation provided in the Appendix A.2.2.

4.3.2 Error Analysis. In step (1) of the quantization algorithm, we create a histogram using the log-space projection approach in DDSketch, which provides a configurable α -relative error bound. In Proposition 4.1, we show that this approach allows us to provide a configurable error guarantee for our approximate K-Means clustering algorithm that is related to α .

Let $X = \{x_1, \dots, x_n\}$ and $\tilde{X} = \{\tilde{x}_1, \dots, \tilde{x}_n\}$ denote a set of n points where $x_i, \tilde{x}_i \in [0, 1]$ and for all i , $|x_i - \tilde{x}_i| \leq \alpha x_i$ for some $\alpha \in (0, 1)$. Let $M = \{\mu_1, \dots, \mu_k\}$ be the cluster centers of X and the loss of M over inputs X is defined as $L(M) = \frac{1}{n} \sum_{x \in X} \min_{j=1}^k |x - \mu_j|$. The cluster centers \tilde{M} and loss L_q over \tilde{X} are defined similarly. The optimal loss $L(M^*)$ is the loss of the optimal cluster centers $M^* = \arg \min_M L(M)$. The optimal loss $L_q(\tilde{M}^*)$ and cluster centers \tilde{M}^* over \tilde{X} are defined similarly.

PROPOSITION 4.1. *Given any two sets X, \tilde{X} of n points as defined above such that $|x_i - \tilde{x}_i| \leq \alpha x_i \forall i$. For any $k \geq 1$, the difference between the optimal loss of clusterings over X and \tilde{X} are bounded as,*

$$|L(M^*) - L_q(\tilde{M}^*)| \leq \alpha \quad (1)$$

REMARK 4.1. *The result implies that the difference between optimal loss of K-Means clustering over raw inputs X and its histogram counterpart \tilde{X} is bounded by α . Using this, we can further show that when the clustering is performed with sample-weighted k-means++,*

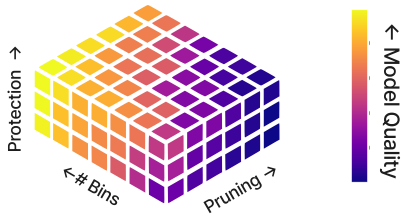


Figure 7: Config Cube: Configuration search space as a function of pruning fraction, protection fraction, and number of bins. The color gradient indicates the direction of higher model quality.

then the expected loss over \tilde{X} is bounded by the optimal loss over X and an additional term related to α^2 . We provide detailed proofs in Appendix A.2.

5 QUANTIZATION CONFIGURATION MANAGER

In this section, we describe the functioning of QUANTIZATION CONFIGURATION MANAGER. This subsystem allows users to specify the maximum acceptable decrease in model quality due to quantization in a single checkpointing operation, measured through a user-defined metric such as loss, accuracy, or perplexity. For each checkpoint instance, the manager aims to identify a quantization configuration that maximizes compression ratio while adhering to the quality threshold.

5.1 Search Space

First, we introduce the quantization configurations that comprise the search space of QUANTIZATION CONFIGURATION MANAGER. Our quantization algorithm possesses four adjustable parameters: pruning fraction, protection fraction, number of quantization bins, and pruning metric, as detailed in Section 4. We list the search range for each configuration knob in Appendix A.3.1.

Previous research on quantization [25, 62, 72, 84, 89] suggests that the quality of quantization can be enhanced by selecting a different number of quantization bins for each layer, based on their sensitivity to quantization. However, this significantly increases the time required for the search process. Therefore, we use the same number of quantization bins across all layers, with the exception of embedding layers. We have observed that embedding layers are considerably more sensitive to quantization, in line with findings from other research on Transformer model quantization [78, 87]. Therefore, we determine the quantization parameters for embedding layers separately, setting the pruning fraction to zero and selecting the number of bins to be either 16 or 32. For all other layers, the number of quantization bins can vary from 4 to 32.

5.2 Search Strategy

Most existing checkpoint compression systems require the user to specify a fixed quantization configuration ahead of time. However, there is no silver bullet when it comes to choosing the right quantization configuration. The optimal configuration depends on the model and the stage of training. For instance, 8-bin quantization might be sufficient early in training, but later stages may necessitate a 16-bin

version when the model is packed with more information. Likewise, models like MobileNet v3 [46], which are parameter-efficient, need more quantization bins compared to models like VGG-19 [79], which have high parameter redundancy. QUANTIZATION CONFIGURATION MANAGER offers a search strategy to dynamically adapt quantization configuration to handle such varying scenarios.

Overview of the Search Algorithm. The naive approach to identifying optimal quantization configuration by evaluating each configuration in the search space is costly – the search space contains over 200 configurations for non-embedding layers. Instead, our search strategy achieves a high-quality configuration with the cost of a single minibatch in the steady state for most workloads. We achieve this by leveraging insight that the optimal quantization configuration remains largely similar between adjacent checkpoints. At the first checkpoint, we perform an exhaustive search to identify the optimal configuration. Subsequently, we greedily select the configuration by only evaluating the configurations that are similar to the previous best configuration. In the unlikely scenario where we can’t identify a configuration that satisfies the quality constraint, we fall back to the exhaustive search. Typically, we observe that we need to resort to exhaustive search at most 2-3 times during the entire span of model training.

Guided Exhaustive Search. We incorporate domain-specific knowledge into the search process to minimize the cost associated with exhaustive search. Consider if we only had one adjustable parameter - the number of quantization bins. We know that model quality increases monotonically with the number of bins, while the compression ratio decreases. In this setting, we can find the optimal number of bins using a variation of binary search. We apply this approach to multiple configuration parameters, arranging three configuration knobs (number of bins, pruning fraction & protection fraction) across three axes of a configuration cube as shown in Figure 7. This arrangement ensures a monotonic increase in model quality across each axis, allowing us to use a divide-and-conquer method. Algorithm 4 provides a sketch of this procedure. We obtain the optimal configuration by repeating this search procedure with the two pruning metrics, magnitude and sensitivity, and selecting the better of the two.

Delta-Neighbourhood Search. In the steady-state, we obtain a suitable configuration by greedily selecting the best configuration within the ϵ -delta neighborhood of the configuration chosen at the previous checkpoint. The ϵ -delta neighborhood is defined as all configurations that are at most ϵ steps away in the configuration cube from the given configuration.

At the outset of each neighborhood search, we assess a configuration that mirrors the previously identified best setup, albeit with an altered pruning metric. The pruning metric is modified only if this results in a noticeable enhancement in the quality of the quantized model. If such an improvement is confirmed, the neighborhood search proceeds with the newly adjusted metric. As training advances, the model’s increasing density and heightened sensitivity to compression make it less amenable to aggressive quantization strategies. In line with this, subsequent neighborhood searches intentionally rule out configurations more aggressive than the prior optimal setting.

5.3 Search Parallelization

We speed up the search by parallelizing the search in distributed data-parallel training workloads. Since each data parallel replica maintains an identical model state, we can parallelize the search process. Configuration search trials are evaluated in groups of m , where m is the degree of data parallelism. While scheduling the trials, we arrange them in a way that allows for an early exit. For instance, in the delta neighborhood search, we order the configurations in decreasing order of compression ratio. If in a given round of evaluation, we find a solution that satisfies the quality constraint, we can exit the search without evaluating the remainder of the configurations. Our experiments show that for a moderate data parallelism degree of eight, a high-quality configuration can be found within a single round of evaluation.

6 DELTA ENCODER: EFFICIENT STORAGE OF QUANTIZED MODELS

To enhance the storage efficiency of compressed models, we introduce a DELTA ENCODER that stores the differences between successive checkpoints. Traditional checkpointing systems don't readily allow for delta encoding because they store data in floating-point format. With quantized models, delta encoding becomes feasible by monitoring changes between quantization buckets rather than exact values.

6.1 Calculating Delta

To compute the delta between the adjacent checkpoints, we first transform quantized values into integers. The delta can then be computed by simply calculating the difference between the quantized integer values of the successive checkpoints for each layer, similar to the scheme proposed in QD-compressor [52], Delta-DNN [47], and LC-checkpoint [13]. Note the values of the delta can be in the range $[Q_{\min} - Q_{\max}, Q_{\min} + Q_{\max}]$ where Q_{\max} and Q_{\min} refer to the maximum and minimum quantized integer values. We employ the technique proposed by Zhang et al. [52] that treats the quantization range as a cyclic buffer to confine delta values within $[Q_{\min}, Q_{\max}]$, which reduces one extra bit for storage. Concretely, for integer-mapped quantized checkpoints C_q^{i-1} and C_q^i , we compute the delta D_i as $D_i = (C_q^{i-1} - C_q^i) \bmod B$, where B is the number of quantization bins. Similarly, C_q^i can be reconstructed as follows, $C_q^i = (C_q^{i-1} - D_i) \bmod B$.

Due to the dynamic changes in the system configuration, the number of quantization bins may vary between checkpoints. We address this by adjusting the size of the cyclic buffer to the maximum number of bins in either checkpoint. Additionally, pruned and protected values in our quantization scheme are treated as unique quantization levels with the same delta calculation. The protected values from checkpoint C^i are stored separately to aid reconstruction.

6.2 Encoding Delta

After delta calculation, we use a combination of run-length encoding [36] and Huffman [49] encoding to reduce its storage footprint. Given that parameter changes are minimal in the later training

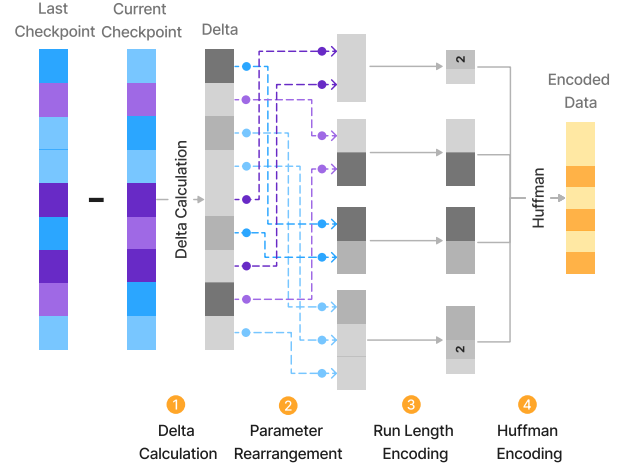


Figure 8: Delta Encoding Pipeline: rearrange and split computed delta based on the quantization bucket each parameter belonged to in the last checkpoint.

stages, run-length encoding is particularly effective for compression. Standard run-length encoding can incur significant overhead due to the values with a run-length of one. We can reduce this overhead by only storing the run-lengths only when it is greater than one. However, this requires a mechanism to distinguish between the encoded values and their run-lengths. We achieve this by simply negating the sign of all the values, such that all the run-lengths are positive while all delta values are less than or equal to zero. Huffman encoding is then applied to the run-length encoded data for further compression.

6.3 Parameter Rearrangement for Efficient Encoding

The efficiency of run-length encoding depends on the arrangement of the parameters. We observe that the migration rate (i.e., the fraction of parameters that change the quantization bucket between adjacent checkpoints) of parameters can differ significantly between different quantization buckets. In the default arrangement where parameters of all quantization buckets are interleaved, the run-lengths get interrupted by the buckets with high migration rates, resulting in poor compression ratios.

To prevent this, we rearrange parameters to isolate the parameters from different quantization buckets. After calculating the delta, we split delta values corresponding to each quantization bucket in the source checkpoint into separate groups, as shown in the second step of Figure 8. Each group is then encoded separately. This ensures that quantization bins with high migration rates don't affect others. The process can easily be reversed during reconstruction and does not require any additional storage to obtain the parameter arrangement. We provide the full algorithm in Appendix B.1. The approach is particularly useful when the number of quantization bins changes between checkpoints. As demonstrated in Section 9.3, this optimization can significantly improve the compression ratio.


```

from dynaquant import CompressorRegistry
# Before train loop
compressor = CompressorRegistry.get_compressor(
    system, model, eval_batches, search_config, search_metric,
    threshold)
...
while global_step < max_training_steps:
    ...
    # Inside train loop
    if should_checkpoint(global_step):
        compressor.compress(global_step)
    ...
    # Before flushing gradients
    compressor.before_gradient_flush()
    optimizer.zero_grad()
    ...
    # After backwards pass
    compressor.on_backward_pass_end()
    optimizer.step()
    ...

```

Listing 1: DynaQuant API usage with native Pytorch applications

```

from composer import Trainer
from dynaquant.integrations.composer import DynaQuantCallback
# Add DynaQuant to list of callbacks
trainer = Trainer(
    ...
    callbacks=[DynaQuantCallback()],
)
trainer.fit()

```

Listing 2: MosaicML Composer application with DynaQuant callback integration.

7 IMPLEMENTATION

We have developed DynaQuant and all the baseline systems discussed in Section 8 using Pytorch, amounting to 7377 lines of Python code. To enhance the performance of delta encoding, we have implemented Huffman encoding and run-length encoding using 300 lines of C++ code. DynaQuant can be effortlessly integrated into user applications with less than 10 lines of code modifications (Listing 1). Additionally, we provide a custom callback for the MosaicML composer [68] library, enabling single-line integration of our system into applications developed with Composer (Listing 2). This strategy can be readily extended to similar frameworks such as Pytorch-lightning [30] and Keras [15], both of which offer a high-level trainer interface.

8 EVALUATION SETUP

In this section, we describe the setup used in our evaluations. Our experimental environment comprises servers equipped with 8 NVIDIA A40s GPUs connected with peer-wise NVLINK, 128 AMD CPU cores, and 504 GB memory.

8.1 Evaluation Criteria

We compare checkpoint compression systems along the following three metrics:

Storage Efficiency. We report the end-to-end compression ratio, calculated by comparing the total size of compressed model checkpoints to their uncompressed counterparts.

Model Quality. We compare the quality of machine learning models trained from compressed checkpoints against a baseline model trained without checkpoint compression. Model quality is evaluated

Model	Architecture	Task	Parameters
ResNet18 [44]	ConvNet	Vision	11.7 M
ResNet50 [44]	ConvNet	Vision	25.6 M
ResNet152 [44]	ConvNet	Vision	60.2 M
MobileNet V3 Large [46]	ConvNet	Vision	5.5 M
VGG19 [79]	ConvNet	Vision	143.7 M
ViT B32 [26]	Transformer	Vision	88.2 M
ViT L32 [26]	Transformer	Vision	306.5 M
BERT Base [22]	Transformer	Language	110 M
BERT Large [22]	Transformer	Language	345 M
GPT-2 Medium [73]	Transformer	Language	335 M
Pythia 1B [9]	Transformer	Language	1 B

Table 2: Summary of models used in the evaluation.

by relative quality degradation on accuracy or loss. For instance, if the baseline achieves 77.5% accuracy and training from compressed checkpoints results in 77.4% accuracy, the relative quality degradation is computed as, $\frac{77.5-77.4}{77.5} * 100\% = 0.13\%$.

Runtime Overhead. We compare compression techniques based on their runtime overhead, measured as time spent on compression as a fraction of the total training time.

8.2 Evaluation Scenarios, Models and Datasets

We evaluate DynaQuant across 7 different model families, encapsulating tasks in both vision and language modeling. These models vary in complexity, with the number of parameters ranging from 5.5 million to 1 billion. Details on all models and datasets used are reported in Table 2 and Table 11.

We evaluate DynaQuant for two use cases: fault-tolerant training and transfer learning.

Fault-tolerant Training. In this scenario, we simulate multiple failures during the training process and perform the recovery using compressed checkpoints. Our evaluation involves four models: ResNet-152 [44], ViT-32L [26], BERT Base [22], and GPT2 Medium [73]. The first two, representing the vision models, are trained on the Imagenet 1K [20] datasets for classification tasks. The latter two, BERT and GPT models, undergo training for language modeling tasks using C4 [74] and OpenWebText [35] datasets, respectively. Training of GPT2 Medium and ViT-32L requires ≈ 650 NVIDIA A40 GPU hours. Kaplan et al. [55] show that larger models require proportionally larger compute time for training. Due to limited compute access at our disposal, we leave experiments with larger model sizes for future work. The implementation details and hyper-parameters used for training are provided in Appendix C.2.

Transfer Learning. In these experiments, we perform transfer learning tasks by training from a compressed checkpoint of pre-trained models. We use BERT Large [22] and Pythia [9] models for transfer learning experiments. Specifically, the BERT model is fine-tuned on GLUE [83] tasks, STS-B, SST-2, and MNLI, while the Pythia model is fine-tuned using the Alpaca [81] instruction-following dataset.

8.3 Baseline Systems

We benchmark the performance of DynaQuant against three state-of-the-art checkpoint compression systems, Check-N-Run [27], QD-compressor [52], and GOBO [87]. We reimplemented all three

baseline systems due to a lack of openly accessible functional implementations. We extended all the baseline systems to support for GPU-accelerated implementation of their quantization algorithms. We also added configuration search capability (search space defined in Appendix A.3.1) for these systems.

- **QD+**: Our implementation of QD-compressor [52], which uses an entropy-based variable bit-width uniform quantization scheme. We address an oversight in the original description which restricted the applicability of the delta compression algorithm to cases where the number of bins assigned to a layer changes between successive checkpoints.
- **GOBO+**: Our implementation of GOBO [87]. While GOBO was originally proposed for post-training quantization, we implement it within theDynaQuant framework to allow in-training compression. We also modify the GOBO clustering algorithm to include a soft termination condition which significantly reduces the runtime.
- **CNR+**: Our implementation of Check-N-Run [27]. Since Check-N-Run was originally developed with the intent to support deep learning recommendation models, the delta compression algorithm proposed in the system cannot be used for regular deep learning workloads. Thus we only implement the quantization algorithm [37] used by Check-N-Run for comparison.

9 EVALUATION

In this section, we evaluate the empirical performance of our checkpoint compression system DynaQuant. Experiments show that:

- DynaQuant achieves up to 26-39 \times overall compression ratio and less than 0.6% runtime overhead in fault-tolerance training, consistently offering the best accuracy-storage tradeoff compared to alternatives. Even with as many as 20 restores from compressed checkpoints, we achieve less than 1.1% end-to-end relative model quality degradation (§ 9.1).
- DynaQuant achieves better or similar performance on downstream transfer learning tasks using compressed checkpoints that are 10 \times smaller than the size of the pre-trained models, outperforming the closest state-of-the-art compression system by 2 \times (§ 9.2).
- DynaQuant’s non-uniform quantization algorithm and delta encoding scheme contribute meaningfully to the overall performance (§ 9.3).

9.1 End-to-end Evaluation: Fault-Tolerant Training using Compressed Checkpoints

To evaluate the impact of employing compressed checkpoints for fault-tolerant training, we conduct end-to-end training of four models under simulated failure conditions. Each experiment has 10 evenly distributed failures (every 3-8 hours of training) throughout the training duration. All models are trained using data parallelism across 8 NVIDIA A40 GPUs, with the largest models taking 3.5 days to train. We exclude GOBO+ because it fails to meet performance overhead requirements. For more details see Section 9.3.

We first analyze the trade-off between storage overhead and end-to-end model quality under different per-checkpoint error thresholds. Figure 10 shows results for ResNet-152 training. With a 1% per-checkpoint threshold, we achieve 21.82 \times compression,

with no end-to-end quality degradation. At a 5% per-checkpoint threshold, there is a small end-to-end relative accuracy drop (0.5%) while the compression ratio goes up to 39.09 \times . For all thresholds, DynaQuant demonstrates an end-to-end degradation of less than 1% and achieves a better compression-quality threshold when compared to CNR+ and QD+. Notably, CNR and QD+ struggle to reach high compression ratios.

Figure 10b demonstrates how the number of restores in the training runs for ResNet152 impacted the end-to-end quality. Even with 20 restores, which is equivalent to a restore every 4.5 epochs, the relative error is 1.1% while it drops to 0.16% for 5 restores. Under high rates of simulated failure, DynaQuant maintains robust end-to-end model quality.

	System	Deg. % (\downarrow)	CR (\uparrow)	Overhead % (\downarrow)
ResNet-152 (Base Acc: 77.41%)	CNR+	0.36	5.71	0.61
	QD+	-0.09	11.82	0.11
	Ours	0.50	39.09	0.35
ViT L32 (Base Acc: 71.36%)	CNR+	-0.21	7.82	0.96
	QD+	0.12	16.31	0.18
	Ours	-0.46	26.19	0.51
BERT Base (Base Acc: 68.49%)	CNR+	3.97	6.78	1.03
	QD+	\times	\times	\times
	Ours	0.80	29.25	0.58
GPT-2 Medium (Base Loss: 2.72)	CNR+	0.25	6.35	0.55
	QD+	1.10	22.15	0.10
	Ours	0.61	29.81	0.32

Table 3: Performance of checkpoint compression systems on failure recovery task. Deg. % = Relative quality degradation, CR = Overall compression ratio, Overhead % = Percentage of training time spent on compression.

For our experiments on BERT Base, ViT L32, and GPT-2 Medium, we fixed the per-checkpoint quality degradation threshold at 5%. As Table 3 reveals, DynaQuant achieves between 26-39 \times reduction in storage requirements across various model families, marking a 3.5-6.5 \times improvement over CNR+, and 1.3-3.3 \times improvement over QD+. This is achieved while keeping the end-to-end relative degradation on the final quality metric below 1%, and the checkpointing overhead of our system remains less than 0.6% of the total training time, as shown in Table 3.

While QD+ achieves a higher compression ratio compared to CNR+ due to its delta compression ability, we find the quality of models generated by the system to be inconsistent. In particular, we see a large drop in accuracy (to 4.43%) after 8 restores for BERT-Base training. We observe similarly inconsistent behavior from QD+ in our quantization ablation studies (Section 9.3.1).

Due to our local error threshold-based search policy, the end-to-end model quality remains preserved even with as many as 20 restores from compressed checkpoints. In some cases, like ViT-L32, we observe that restoring from compressed checkpoints can act as a regularization mechanism, and result in better end-to-end performance.

DynaQuant’s delta encoding scheme is particularly effective during the later stages of training when model updates decelerate. We note peak delta compression performances of above 100 \times across all models. Figure 9 delineates the compression ratio at each checkpoint. Note that the peaks in the compression ratio seen in the

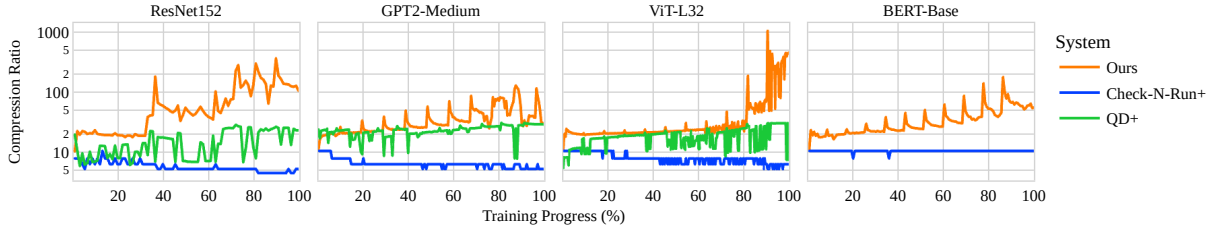


Figure 9: Compression ratio at every checkpoint during the training of various models.

Model	Mean Number of Quantization Bins (\downarrow)											
	0.1% Degradation				1% Degradation				5% Degradation			
	CNR+	QD+	GOBO+	Ours	CNR+	QD+	GOBO+	Ours	CNR+	QD+	GOBO+	Ours
ResNet18	42.84	×	×	21.25	33.75	35.51	33.12	16.85	23.55	23.25	17.50	10.19
ResNet50	46.36	×	×	21.39	35.07	53.65	31.78	14.36	23.06	33.69	20.12	8.24
ResNet152	59.32	×	×	20.18	40.71	×	×	11.92	26.74	39.36	×	7.20
MobileNet V3 Large	65.24	×	×	27.92	54.44	×	×	32.48	36.68	47.96	30.79	17.91
VGG19	50.46	×	×	13.06	31.01	45.36	×	8.99	18.48	25.15	×	6.26
ViT B32	37.01	×	×	19.88	28.37	38.43	×	14.33	20.85	28.79	×	9.75
ViT L32	37.40	×	×	13.31	32.95	×	×	10.79	25.36	35.34	×	8.46
BERT Base	×	×	×	54.30	81.45	×	×	22.75	43.18	53.10	×	12.74
GPT-2 Medium	106.86	×	×	54.71	47.71	60.17	×	16.19	24.60	31.14	×	9.08

Table 4: One-shot compression performance under quality degradation constraints. We consider the mean number of quantization bins required to achieve the quality degradation constraint across ten evenly spaced checkpoints during training. System timeouts (30 mins for each evaluation of each configuration) are represented by \times , while scenarios, where no suitable configuration is found, are marked by \times .

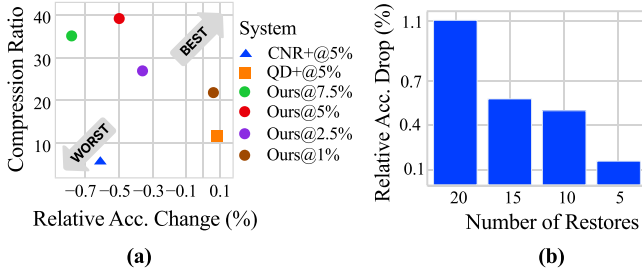


Figure 10: End-to-end relative quality degradation for ResNet152 fault-tolerant training. (a) Comparison between baseline systems and DynaQuant with varying per-checkpoint thresholds. (b) Impact of the number of checkpoint restores for DynaQuant.

plots correspond to checkpoints directly following restores from the compressed state.

Model	Runtime in Milliseconds (\downarrow)			
	Quantile		Clustering (K=32)	
	CuPy [70]	Ours	CuML [75]	Ours
ResNet152	71.9	15.2	10200	1160
ViT L32	364	80.9	50100	1140
BERT Base	155	33.9	20700	411
GPT-2 Medium	390	86.2	53400	819

Table 5: Runtime cost of various operations in DynaQuant compared with standard off-the-shelf implementations.

9.2 End-to-end Evaluation: Transfer Learning from Compressed Checkpoints

In this subsection, we assess the efficacy of utilizing compressed checkpoints for transfer learning tasks.

Model	Task	Metric	Baseline	CNR+	QD+	Ours
BERT Large	SST-2	CR (\uparrow)	-	4.57	4.00	11.32
		Acc (\uparrow)	93.2	92.9	93.0	93.3
	MNLI	Acc (\uparrow)	85.9	86.0	86.0	85.9
		PC (\uparrow)	86.1	87.6	87.8	88.3
Pythia 1B	Alpaca	CR (\uparrow)	-	5.33	4.57	9.99
		CE (\downarrow)	0.894	0.910	0.906	0.919

Table 6: Performance of checkpoint compression systems on the transfer learning task. CR = Compression ratio, Acc = Accuracy, PC = Pearson correlation, CE = Cross-entropy Loss.

For these experiments, we perform the compression process on pre-trained model checkpoints, then deploy the compressed models for downstream task fine-tuning. We evaluate the BERT-Base and Pythia 1B models on a suite of downstream tasks. The results for all three fine-tuning tasks are consolidated in Table 6. The checkpoints used for this experiment are obtained by setting a 5% quality degradation threshold. We observe that for both the models, DynaQuant can achieve compression ratios up to 11 \times even without delta encoding, 2 \times higher compared to other systems. Notably, we find that the use of compressed checkpoints does not harm the performance of the downstream model, and we achieve performance comparable to baseline across all tasks and models.

9.3 Microbenchmarks & Ablation Studies

9.3.1 Non-uniform Quantization. We evaluate the compression quality and the runtime of our non-uniform quantization approach.

We compare various quantization algorithms on their ability to optimize compression while maintaining model quality. To perform this experiment, we collect ten evenly spaced checkpoints for various models during their training. For each quantization technique, we compute the minimum number of quantization bins required to

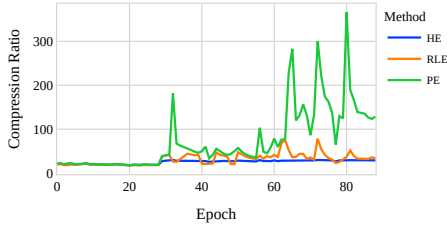


Figure 11: Performance of various delta encoding schemes for checkpointing during ResNet-152 training. HE = Huffman Encoding, RLE = Run Length Encoding + Huffman Encoding, PE = Parameter Rearrangement-based Encoding.

achieve error thresholds of 0.1%, 1%, and 5% at each checkpoint and report the mean number of bins across all checkpoints. We disable parameter pruning in our system for this experiment to allow for easier comparison. The results are presented in Table 4. We observe that DynaQuant achieves consistently superior performance across all the models and quality thresholds. On the other hand, GOBO+, which implements a variant of the k-means clustering algorithm for quantization, times out (30 mins+) for models with more than 30 million parameters. QD+ fails to find valid quantization configurations for strict quality degradation thresholds. Among baseline systems, only CNR+ manages to constantly find quantization configurations that satisfy the quality thresholds. However, it requires a 2-4 \times higher number of quantization bins to achieve the same quality as DynaQuant due to their use of uniform quantization schemes.

Next, we evaluate the runtime performance of our quantization algorithm. There are two key compute operations in our quantization process: computing qualities for pruning and protection, and the K-Means clustering for quantization. We implement our approach in Pytorch [71] with support for both CPU and GPU execution. We compare the performance of our implementation against off-the-shelf GPU-enabled implementations for quantile estimation in CuPy [70] and K-Means clustering in CuML [75] respectively. The results are reported in Table 5. Our quantile estimation algorithm achieves 3-4 \times higher performance compared to CuPy, while we note a speed-up of up to 65 \times in quantile computation.

9.3.2 Parameter Rearrangement-based Delta Encoding. The key optimization in DynaQuant’s delta encoding scheme is parameter rearrangement, which enables it to decrease the entropy in each compressed chunk. To assess the contribution of this optimization, we compare three variants of our delta encoding scheme: the Huffman encoding variant used in QD+ (HE), run-length plus Huffman encoding (RLE), and parameter rearrangement-based delta encoding (PE) on the ResNet-152 training job. The results are illustrated in Figure 11. With parameter rearrangement, we achieve much higher compression in the later phase of training. Notably, we obtain a maximum compression ratio of 366 with rearrangement compared to 79 with RLE and 30 with HE. This translates to overall lower storage overhead. The Huffman and run-length encoding-based schemes only achieve overall storage overhead reduction of 25 \times and 28 \times respectively, as opposed to 39 \times with parameter rearrangement.

10 RELATED WORK

Previously, several studies [13, 27, 47, 52] have examined compression techniques in the context of model checkpointing systems. These systems use a combination of model quantization and delta encoding to reduce the storage overhead by leveraging high similarity between adjacent checkpoints. Every compressed checkpoint only stores the differences accumulated since the previous checkpoint. The final checkpoint state can be reconstructed by iteratively applying the delta values to the initial checkpoint.

We discuss the compression techniques used in prior works below. LC-Checkpoint [13] uses an exponent-based non-uniform quantization scheme, while Delta-DNN [47] proposes a uniform quantization approach with a configuration search strategy to limit the quantization error. However, these methods achieve a lower compression performance compared to methods utilizing more sophisticated quantization approaches. QD-Compressor [52] uses an entropy-based variable bit-width uniform quantization scheme. While the authors propose a delta encoding algorithm, it does not consider the changes in quantization bit widths induced by their variable bit-width technique, rendering the delta compression subsystem impractical. Check-N-Run [27] is a more recent system that addresses checkpoint compression for large deep recommendation models. It applies an adaptive uniform quantization method [37] along with a delta compression scheme specifically designed for recommendation models. Unfortunately, several mechanisms proposed in Check-N-Run, including the delta compression algorithm, are not suitable for traditional deep learning models, which limits its overall utility.

11 CONCLUSION

DynaQuant introduces a method for algorithmically transparent in-training checkpoint compression, enabled by a fast non-uniform quantization scheme. Additionally, DynaQuant employs a quantization-aware delta compression algorithm, using parameter rearrangement to enhance storage efficiency. The framework can be applied in various contexts requiring model checkpoints, such as fault-tolerant distributed machine learning and transfer learning. By integrating non-uniform quantization, automatic quantization search space management, and delta compression, we show that DynaQuant can reduce checkpoint storage requirements by 26-39 \times , outperforming existing methods by 1.3-3.3 \times , while addressing the quality consistency issues in existing systems. In our experiments, DynaQuant demonstrates the ability to induce a tradeoff space between the end-to-end model quality and checkpoint storage overhead, achieving up to 10 \times compression without loss in model quality.

REFERENCES

- [1] 2022. OPT 175B Training Logbook. https://github.com/facebookresearch/metaseq/blob/main/projects/OPT/chronicles/OPT175B_Logbook.pdf
- [2] 2023. bert-base-uncased · Hugging Face. <https://huggingface.co/bert-base-uncased>
- [3] 2023. Hugging Face. <https://huggingface.co>
- [4] 2023. MosaicML BERT. <https://www.mosaicml.com/blog/mosaicbert>
- [5] Margareta Ackerman and Shai Ben-David. 2009. Clusterability: A theoretical study. In *Artificial intelligence and statistics*. PMLR, 1–8.
- [6] David Arthur and Sergei Vassilvitskii. 2007. K-means++ the advantages of careful seeding. In *Proceedings of the eighteenth annual ACM-SIAM symposium on Discrete algorithms*. 1027–1035.

- [7] Ron Banner, Yury Nahshan, and Daniel Soudry. 2019. Post training 4-bit quantization of convolutional networks for rapid-deployment. *Advances in Neural Information Processing Systems* 32 (2019).
- [8] Shai Ben-David and Nika Haghtalab. 2014. Clustering in the presence of background noise. In *International Conference on Machine Learning*. PMLR, 280–288.
- [9] Stella Biderman, Hailey Schoelkopf, Quentin Anthony, Herbie Bradley, Kyle O’Brien, Eric Hallahan, Mohammad Aflah Khan, Shivanshu Purohit, USVSN Sai Prashanth, Edward Raff, et al. 2023. Pythia: A suite for analyzing large language models across training and scaling. *arXiv preprint arXiv:2304.01373* (2023).
- [10] Tom Brown, Benjamin Mann, Nick Ryder, Melanie Subbiah, Jared D Kaplan, Prafulla Dhariwal, Arvind Neelakantan, Pranav Shyam, Girish Sastry, Amanda Askell, et al. 2020. Language models are few-shot learners. *Advances in neural information processing systems* 33 (2020), 1877–1901.
- [11] Yaohui Cai, Zhewei Yao, Zhen Dong, Amir Gholami, Michael W Mahoney, and Kurt Keutzer. 2020. ZeroQ: A novel zero shot quantization framework. In *Proceedings of the IEEE/CVF Conference on Computer Vision and Pattern Recognition*. 13169–13178.
- [12] Zhaowei Cai, Xiaodong He, Jian Sun, and Nuno Vasconcelos. 2017. Deep learning with low precision by half-wave gaussian quantization. In *Proceedings of the IEEE conference on computer vision and pattern recognition*. 5918–5926.
- [13] Yu Chen, Zhenming Liu, Bin Ren, and Xin Jin. 2020. On efficient constructions of checkpoints. *arXiv preprint arXiv:2009.13003* (2020).
- [14] Yoojin Choi, Mostafa El-Khamy, and Jungwon Lee. 2016. Towards the limit of network quantization. *arXiv preprint arXiv:1612.01543* (2016).
- [15] François Chollet et al. 2015. Keras. <https://keras.io>.
- [16] Yoni Choukroun, Eli Kravchik, Fan Yang, and Pavel Kisilev. 2019. Low-bit quantization of neural networks for efficient inference. In *2019 IEEE/CVF International Conference on Computer Vision Workshop (ICCVW)*. IEEE, 3009–3018.
- [17] Matthieu Courbariaux, Yoshua Bengio, and Jean-Pierre David. 2015. Binaryconnect: Training deep neural networks with binary weights during propagations. *Advances in neural information processing systems* 28 (2015).
- [18] Saurabh Dash and Saibal Mukhopadhyay. 2020. Hessian-driven unequal protection of dnn parameters for robust inference. In *Proceedings of the 39th International Conference on Computer-Aided Design*. 1–9.
- [19] Pau De Jorge, Amartya Sanyal, Harkirat S Behl, Philip HS Torr, Gregory Rogez, and Puneet K Dokania. 2020. Progressive skeletonization: Trimming more fat from a network at initialization. *arXiv preprint arXiv:2006.09081* (2020).
- [20] Jia Deng, Wei Dong, Richard Socher, Li-Jia Li, Kai Li, and Li Fei-Fei. 2009. Imagenet: A large-scale hierarchical image database. In *2009 IEEE conference on computer vision and pattern recognition*. Ieee, 248–255.
- [21] Tim Dettmers, Mike Lewis, Younes Belkada, and Luke Zettlemoyer. 2022. Llm.int8(): 8-bit matrix multiplication for transformers at scale. *arXiv preprint arXiv:2208.07339* (2022).
- [22] Jacob Devlin, Ming-Wei Chang, Kenton Lee, and Kristina Toutanova. 2018. Bert: Pre-training of deep bidirectional transformers for language understanding. *arXiv preprint arXiv:1810.04805* (2018).
- [23] Zhen Dong, Zhewei Yao, Daiyaan Arfeen, Amir Gholami, Michael W Mahoney, and Kurt Keutzer. 2020. HAWQ-V2: Hessian Aware trace-Weighted Quantization of Neural Networks. In *Advances in Neural Information Processing Systems*, H. Larochelle, M. Ranzato, R. Hadsell, M.F. Balcan, and H. Lin (Eds.), Vol. 33. Curran Associates, Inc., 18518–18529. https://proceedings.neurips.cc/paper_files/paper/2020/file/d77c703536718b95308130ff2e5cf9ee-Paper.pdf
- [24] Zhen Dong, Zhewei Yao, Amir Gholami, Michael W Mahoney, and Kurt Keutzer. 2019. Hawq: Hessian aware quantization of neural networks with mixed-precision. In *Proceedings of the IEEE/CVF International Conference on Computer Vision*. 293–302.
- [25] Zhen Dong, Zhewei Yao, Amir Gholami, Michael W Mahoney, and Kurt Keutzer. 2019. Hawq: Hessian aware quantization of neural networks with mixed-precision. In *Proceedings of the IEEE/CVF International Conference on Computer Vision*. 293–302.
- [26] Alexey Dosovitskiy, Lucas Beyer, Alexander Kolesnikov, Dirk Weissenborn, Xiaohua Zhai, Thomas Unterthiner, Mostafa Dehghani, Matthias Minderer, Georg Heigold, Sylvain Gelly, et al. 2020. An image is worth 16x16 words: Transformers for image recognition at scale. *arXiv preprint arXiv:2010.11929* (2020).
- [27] Assaf Eisenman, Kiran Kumar Matam, Steven Ingram, Dheevatsa Mudigere, Raghuraman Krishnamoorthi, Krishnakumar Nair, Misha Smelyanskiy, and Murali Annavaram. 2022. Check-N-Run: a checkpointing system for training deep learning recommendation models. In *19th USENIX Symposium on Networked Systems Design and Implementation (NSDI 22)*. 929–943.
- [28] A.P. Engelbrecht. 2001. A new pruning heuristic based on variance analysis of sensitivity information. *IEEE Transactions on Neural Networks* 12, 6 (2001), 1386–1399. <https://doi.org/10.1109/72.963775>
- [29] Fartash Faghri, Iman Tabrizian, Ilia Markov, Dan Alistarh, Daniel M Roy, and Ali Ramezani-Kebrya. 2020. Adaptive gradient quantization for data-parallel sgd. *Advances in neural information processing systems* 33 (2020), 3174–3185.
- [30] William Falcon et al. 2019. PyTorch Lightning. *GitHub. Note: <https://github.com/PyTorchLightning/pytorch-lightning>* 3 (2019).
- [31] Jun Fang, Ali Shafiee, Hamzah Abdel-Aziz, David Thorsley, Georgios Georgiadis, and Joseph H Hassoun. 2020. Post-training piecewise linear quantization for deep neural networks. In *Computer Vision—ECCV 2020: 16th European Conference, Glasgow, UK, August 23–28, 2020, Proceedings, Part II* 16. Springer, 69–86.
- [32] Jonathan Frankle and Michael Carbin. 2018. The lottery ticket hypothesis: Finding sparse, trainable neural networks. *arXiv preprint arXiv:1803.03635* (2018).
- [33] Pasi Fränti and Sami Sieranoja. 2019. How much can k-means be improved by using better initialization and repeats? *Pattern Recognition* 93 (2019), 95–112. <https://doi.org/10.1016/j.patcog.2019.04.014>
- [34] Trevor Gale, Erich Elsen, and Sara Hooker. 2019. The state of sparsity in deep neural networks. *arXiv preprint arXiv:1902.09574* (2019).
- [35] Aaron Gokaslan and Vanya Cohen. [n.d.]. OpenWebText Corpus.
- [36] Solomon Golomb. 1966. Run-length encodings (corresp.). *IEEE transactions on information theory* 12, 3 (1966), 399–401.
- [37] Hui Guan, Andrey Malevich, Jiyan Yang, Jongsoo Park, and Hector Yuen. 2019. Post-training 4-bit quantization on embedding tables. *arXiv preprint arXiv:1911.02079* (2019).
- [38] Philipp Gysel, Mohammad Motamedi, and Soheil Ghiasi. 2016. Hardware-oriented approximation of convolutional neural networks. *arXiv preprint arXiv:1604.03168* (2016).
- [39] Song Han, Huizi Mao, and William J Dally. 2015. Deep compression: Compressing deep neural networks with pruning, trained quantization and Huffman coding. *arXiv preprint arXiv:1510.00149* (2015).
- [40] Song Han, Jeff Pool, John Tran, and William Dally. 2015. Learning both weights and connections for efficient neural network. *Advances in neural information processing systems* 28 (2015).
- [41] Song Han, Jeff Pool, John Tran, and William Dally. 2015. Learning both Weights and Connections for Efficient Neural Network. In *Advances in Neural Information Processing Systems*, C. Cortes, N. Lawrence, D. Lee, M. Sugiyama, and R. Garnett (Eds.), Vol. 28. Curran Associates, Inc. https://proceedings.neurips.cc/paper_files/paper/2015/file/ae0eb3eed39d2bcef4622b2499a05fe6-Paper.pdf
- [42] Babak Hassibi and David Stork. 1992. Second order derivatives for network pruning: Optimal brain surgeon. *Advances in neural information processing systems* 5 (1992).
- [43] Babak Hassibi, David G Stork, and Gregory J Wolff. 1993. Optimal brain surgeon and general network pruning. In *IEEE international conference on neural networks*. IEEE, 293–299.
- [44] Kaiming He, Xiangyu Zhang, Shaoqing Ren, and Jian Sun. 2015. Deep residual learning for image recognition. *arXiv 2015. arXiv preprint arXiv:1512.03385* 14 (2015).
- [45] Xiangyu He and Jian Cheng. 2018. Learning Compression from Limited Unlabeled Data. In *Proceedings of the European Conference on Computer Vision (ECCV)*.
- [46] Andrew Howard, Mark Sandler, Grace Chu, Liang-Chieh Chen, Bo Chen, Mingxing Tan, Weijun Wang, Yukun Zhu, Ruoming Pang, Vijay Vasudevan, et al. 2019. Searching for mobilenetv3. In *Proceedings of the IEEE/CVF international conference on computer vision*. 1314–1324.
- [47] Zhenbo Hu, Xiangyu Zou, Wen Xia, Sian Jin, Dingwen Tao, Yang Liu, Weizhe Zhang, and Zheng Zhang. 2020. Delta-DNN: Efficiently compressing deep neural networks via exploiting floats similarity. In *Proceedings of the 49th International Conference on Parallel Processing*. 1–12.
- [48] Itay Hubara, Matthieu Courbariaux, Daniel Soudry, Ran El-Yaniv, and Yoshua Bengio. 2016. Binarized Neural Networks. In *Advances in Neural Information Processing Systems*, D. Lee, M. Sugiyama, U. Luxburg, I. Guyon, and R. Garnett (Eds.), Vol. 29. Curran Associates, Inc. https://proceedings.neurips.cc/paper_files/paper/2016/file/d8330f857a17c53d217014ee776bfd50-Paper.pdf
- [49] David A Huffman. 1952. A method for the construction of minimum-redundancy codes. *Proceedings of the IRE* 40, 9 (1952), 1098–1101.
- [50] Benoit Jacob, Skirmantas Kligys, Bo Chen, Menglong Zhu, Matthew Tang, Andrew Howard, Hartwig Adam, and Dmitry Kalenichenko. 2018. Quantization and training of neural networks for efficient integer-arithmetic-only inference. In *Proceedings of the IEEE conference on computer vision and pattern recognition*. 2704–2713.
- [51] Myeongjae Jeon, Shivaram Venkataraman, Amar Phanishayee, Junjie Qian, Wencong Xiao, and Fan Yang. 2019. Analysis of Large-Scale Multi-Tenant GPU Clusters for DNN Training Workloads. In *USENIX Annual Technical Conference*. 947–960.
- [52] Haoyu Jin, Donglei Wu, Shuyu Zhang, Xiangyu Zou, Sian Jin, Dingwen Tao, Qing Liao, and Wen Xia. 2023. Design of a Quantization-Based DNN Delta Compression Framework for Model Snapshots and Federated Learning. *IEEE Transactions on Parallel and Distributed Systems* 34, 3 (2023), 923–937. <https://doi.org/10.1109/TPDS.2022.3230840>
- [53] Prad Kadambi, Karthikeyan Natesan Ramamurthy, and Visar Berisha. 2020. Comparing fisher information regularization with distillation for dnn

- quantization. In *NeurIPS 2020 Workshop: Deep Learning through Information Geometry*.
- [54] Dhiraj Kalamkar, Dheevatsa Mudigere, Naveen Mellempudi, Dipankar Das, Kunal Banerjee, Sasikanth Avancha, Dharma Teja Vooturi, Nataraj Jammalamadaka, Jianyu Huang, Hector Yuen, et al. 2019. A study of BFLOAT16 for deep learning training. *arXiv preprint arXiv:1905.12322* (2019).
- [55] Jared Kaplan, Sam McCandlish, Tom Henighan, Tom B Brown, Benjamin Chess, Rewon Child, Scott Gray, Alec Radford, Jeffrey Wu, and Dario Amodei. 2020. Scaling laws for neural language models. *arXiv preprint arXiv:2001.08361* (2020).
- [56] Karpathy. [n.d.]. Karpathy/nanogpt: The simplest, fastest repository for training/finetuning medium-sized gpts. <https://github.com/karpathy/nanoGPT>
- [57] Yann LeCun, John Denker, and Sara Solla. 1989. Optimal brain damage. *Advances in neural information processing systems* 2 (1989).
- [58] Yann LeCun, John Denker, and Sara Solla. 1989. Optimal brain damage. *Advances in neural information processing systems* 2 (1989).
- [59] Namhoon Lee, Thalaiyasingam Ajanthan, and Philip HS Torr. 2018. Snip: Single-shot network pruning based on connection sensitivity. *arXiv preprint arXiv:1810.02340* (2018).
- [60] Guiying Li, Chao Qian, Chunhui Jiang, Xiaofen Lu, and Ke Tang. 2018. Optimization based layer-wise magnitude-based pruning for DNN compression. In *IJCAI*. 2383–2389.
- [61] Zhouhan Lin, Matthieu Courbariaux, Roland Memisevic, and Yoshua Bengio. 2015. Neural networks with few multiplications. *arXiv preprint arXiv:1510.03009* (2015).
- [62] Hongyang Liu, Sara Elkerdawy, Nilanjan Ray, and Mostafa Elhoushi. 2021. Layer importance estimation with imprinting for neural network quantization. In *Proceedings of the IEEE/CVF Conference on Computer Vision and Pattern Recognition*. 2408–2417.
- [63] TorchVision maintainers and contributors. 2016. *TorchVision: PyTorch’s Computer Vision library*.
- [64] Charles Masson, Jee E Rim, and Homin K Lee. 2019. DDSketch: A fast and fully-mergeable quantile sketch with relative-error guarantees. *arXiv preprint arXiv:1908.10693* (2019).
- [65] Daisuke Miyashita, Edward H Lee, and Boris Murmann. 2016. Convolutional neural networks using logarithmic data representation. *arXiv preprint arXiv:1603.01025* (2016).
- [66] Jayashree Mohan, Amar Phanishayee, and Vijay Chidambaram. 2021. CheckFreq: Frequent, Fine-Grained DNN Checkpointing. In *FAST*, Vol. 21. 203–216.
- [67] Pavlo Molchanov, Stephen Tyree, Tero Karras, Timo Aila, and Jan Kautz. 2016. Pruning convolutional neural networks for resource efficient inference. *arXiv preprint arXiv:1611.06440* (2016).
- [68] Mosaicml. [n.d.]. Mosaicml composer: Train neural networks up to 7x faster. <https://github.com/mosaicml/composer>
- [69] Bogdan Nicolaie, Jiali Li, Justin M. Wozniak, George Bosilca, Matthieu Dorier, and Franck Cappello. 2020. DeepFreeze: Towards Scalable Asynchronous Checkpointing of Deep Learning Models. In *2020 20th IEEE/ACM International Symposium on Cluster, Cloud and Internet Computing (CCGRID)*. 172–181. <https://doi.org/10.1109/CCGrid49817.2020.00-76>
- [70] Ryosuke Okuta, Yuya Unno, Daisuke Nishino, Shohei Hido, and Crissman Loomis. 2017. CuPy: A NumPy-Compatible Library for NVIDIA GPU Calculations. In *Proceedings of Workshop on Machine Learning Systems (LearningSys) in The Thirty-first Annual Conference on Neural Information Processing Systems (NIPS)*. http://learningsys.org/nips17/assets/papers/paper_16.pdf
- [71] Adam Paszke, Sam Gross, Francisco Massa, Adam Lerer, James Bradbury, Gregory Chanan, Trevor Killeen, Zeming Lin, Natalia Gimelshein, Luca Antiga, Alban Desmaison, Andreas Kopf, Edward Yang, Zachary DeVito, Martin Raison, Alykhan Tejani, Sasank Chilamkurthy, Benoit Steiner, Lu Fang, Junjie Bai, and Soumith Chintala. 2019. PyTorch: An Imperative Style, High-Performance Deep Learning Library. In *Advances in Neural Information Processing Systems* 32. Curran Associates, Inc., 8024–8035. <http://papers.neurips.cc/paper/9015-pytorch-an-imperative-style-high-performance-deep-learning-library.pdf>
- [72] Zhongnan Qu, Zimu Zhou, Yun Cheng, and Lothar Thiele. 2020. Adaptive loss-aware quantization for multi-bit networks. In *Proceedings of the IEEE/CVF Conference on Computer Vision and Pattern Recognition*. 7988–7997.
- [73] Alec Radford, Jeffrey Wu, Rewon Child, David Luan, Dario Amodei, Ilya Sutskever, et al. 2019. Language models are unsupervised multitask learners. *OpenAI blog* 1, 8 (2019), 9.
- [74] Colin Raffel, Noam Shazeer, Adam Roberts, Katherine Lee, Sharan Narang, Michael Matena, Yanqi Zhou, Wei Li, and Peter J. Liu. 2019. Exploring the Limits of Transfer Learning with a Unified Text-to-Text Transformer. *arXiv e-prints* (2019). arXiv:1910.10683
- [75] Sebastian Raschka, Joshua Patterson, and Corey Nolet. 2020. Machine Learning in Python: Main developments and technology trends in data science, machine learning, and artificial intelligence. *arXiv preprint arXiv:2002.04803* (2020).
- [76] Mohammad Rastegari, Vicente Ordonez, Joseph Redmon, and Ali Farhadi. 2016. Xnor-net: Imagenet classification using binary convolutional neural networks. In *Computer Vision—ECCV 2016: 14th European Conference, Amsterdam, The Netherlands, October 11–14, 2016, Proceedings, Part IV*. Springer, 525–542.
- [77] Maying Shen, Pavlo Molchanov, Hongxu Yin, and Jose M Alvarez. 2022. When to prune? a policy towards early structural pruning. In *Proceedings of the IEEE/CVF Conference on Computer Vision and Pattern Recognition*. 12247–12256.
- [78] Sheng Shen, Zhen Dong, Jiayu Ye, Linjian Ma, Zhewei Yao, Amir Gholami, Michael W Mahoney, and Kurt Keutzer. 2020. Q-bert: Hessian based ultra low precision quantization of bert. In *Proceedings of the AAAI Conference on Artificial Intelligence*, Vol. 34. 8815–8821.
- [79] Karen Simonyan and Andrew Zisserman. 2014. Very deep convolutional networks for large-scale image recognition. *arXiv preprint arXiv:1409.1556* (2014).
- [80] Shyam A Tailor, Javier Fernandez-Marques, and Nicholas D Lane. 2020. Degree-quant: Quantization-aware training for graph neural networks. *arXiv preprint arXiv:2008.05000* (2020).
- [81] Rohan Taori, Ishaan Gulrajani, Tianyi Zhang, Yann Dubois, Xuechen Li, Carlos Guestrin, Percy Liang, and Tatsunori B. Hashimoto. 2023. Stanford Alpaca: An Instruction-following LLaMA model. https://github.com/tatsu-lab/stanford_alpaca.
- [82] Enzo Tagliapietra, Andrea Bragagnolo, Francesco Odierna, Attilio Fianrotti, and Marco Grangetto. 2022. SeReNe: Sensitivity-Based Regularization of Neurons for Structured Sparsity in Neural Networks. *IEEE Transactions on Neural Networks and Learning Systems* 33, 12 (2022), 7237–7250. <https://doi.org/10.1109/TNNLS.2021.3084527>
- [83] Alex Wang, Amanpreet Singh, Julian Michael, Felix Hill, Omer Levy, and Samuel R Bowman. 2018. GLUE: A multi-task benchmark and analysis platform for natural language understanding. *arXiv preprint arXiv:1804.07461* (2018).
- [84] Kuan Wang, Zhijian Liu, Yujun Lin, Ji Lin, and Song Han. 2019. Haq: Hardware-aware automated quantization with mixed precision. In *Proceedings of the IEEE/CVF Conference on Computer Vision and Pattern Recognition*. 8612–8620.
- [85] Zhewei Yao, Zhen Dong, Zhangcheng Zheng, Amir Gholami, Jiali Yu, Eric Tan, Leyuan Wang, Qijing Huang, Yida Wang, Michael Mahoney, et al. 2021. Hawq-v3: Dyadic neural network quantization. In *International Conference on Machine Learning*. PMLR, 11875–11886.
- [86] Shixing Yu, Zhewei Yao, Amir Gholami, Zhen Dong, Sehoon Kim, Michael W Mahoney, and Kurt Keutzer. 2022. Hessian-aware pruning and optimal neural implant. In *Proceedings of the IEEE/CVF Winter Conference on Applications of Computer Vision*. 3880–3891.
- [87] Ali Hadi Zadeh, Isak Edo, Omar Mohamed Awad, and Andreas Moshovos. 2020. Gobo: Quantizing attention-based nlp models for low latency and energy efficient inference. In *2020 53rd Annual IEEE/ACM International Symposium on Microarchitecture (MICRO)*. IEEE, 811–824.
- [88] Susan Zhang, Stephen Roller, Naman Goyal, Mikel Artetxe, Moya Chen, Shuohui Chen, Christopher Dewan, Mona Diab, Xian Li, Xi Victoria Lin, et al. 2022. Opt: Open pre-trained transformer language models. *arXiv preprint arXiv:2205.01068* (2022).
- [89] Sijie Zhao, Tao Yue, and Xuemei Hu. 2021. Distribution-aware adaptive multi-bit quantization. In *Proceedings of the IEEE/CVF Conference on Computer Vision and Pattern Recognition*. 9281–9290.
- [90] Cankun Zhong, Yang He, Yifei An, Wing W. Y. Ng, and Ting Wang. 2022. A Sensitivity-based Pruning Method for Convolutional Neural Networks. In *2022 IEEE International Conference on Systems, Man, and Cybernetics (SMC)*. 1032–1038. <https://doi.org/10.1109/SMC53654.2022.9945569>
- [91] Michael Zhu and Suyog Gupta. 2017. To prune, or not to prune: exploring the efficacy of pruning for model compression. *arXiv preprint arXiv:1710.01878* (2017).

A QUANTIZER

A.1 Additional Details for Quantile Computation

Algorithm 2 describes the parallelizable version of DDSketch [64] optimized for GPU execution.

A.2 Additional Details for Approximate K-Means

A.2.1 Proof for Error-bound Guarantees. We restate the notations and propositions here for clarity. Let $X = \{x_1, \dots, x_n\}$ and $\tilde{X} = \{\tilde{x}_1, \dots, \tilde{x}_n\}$ denote a set of n points where $x_i, \tilde{x}_i \in [0, 1]$ and for all i , $|x_i - \tilde{x}_i| \leq \alpha x_i$ for some $\alpha \in (0, 1)$. Let $M = \{\mu_1, \dots, \mu_k\}$ be the cluster centers of X and the loss of M over inputs X is defined as $L(M) = \frac{1}{n} \sum_{x \in X} \min_{\mu \in M} |x - \mu|$. The cluster centers \tilde{M} and loss

Algorithm 2: GetQuantileSketchHistogram

Require: X {Input list}
Require: α {Relative Error Bound}
1: $\gamma \leftarrow (1 + \alpha)/(1 - \alpha)$
2: Define X_q as an empty array
3: **for all** x in X **do**
4: Append $\lceil \log_\gamma(x) \rceil$ to X_q
5: **end for**
6: $(\text{bucket_vals}, \text{bucket_counts}) \leftarrow \text{unique}(X_q)$
7: **return** $\text{bucket_vals}, \text{bucket_counts}$

L_q over \tilde{X} are defined similarly. The optimal loss $L(M^*)$ is the loss of the optimal cluster centers $M^* = \arg \min_M L(M)$. The optimal loss $L_q(\tilde{M}^*)$ and cluster centers \tilde{M}^* over \tilde{X} are defined similarly. Let $\mu_M(i) = \arg \min_\mu |\mu - x_i|$ denote the cluster center in M that is closest to the i th input x_i ($\tilde{\mu}_{\tilde{M}}(i)$ is defined similarly for \tilde{x}_i). Note that the loss $L(\tilde{M})$ over the original inputs X with any clustering \tilde{M} over \tilde{X} is at most α greater than the loss $L_q(\tilde{M})$,

$$\begin{aligned} L_q(\tilde{M}) &= \frac{1}{n} \sum_{i=1}^n |\tilde{\mu}_{\tilde{M}}(i) - \tilde{x}_i| \leq \frac{1}{n} \sum_{i=1}^n (|\tilde{\mu}_{\tilde{M}}(i) - x_i| + \alpha x_i) \\ &= L(\tilde{M}) + \frac{\alpha}{n} \sum_{i=1}^n x_i \leq L(\tilde{M}) + \alpha \end{aligned}$$

where the first inequality follows from triangle inequality and the second follows from the fact that $\frac{1}{n} \sum_{i=1}^n x_i \leq 1$. Using similar arguments, one can verify that $L(\tilde{M}) \leq L_q(\tilde{M}) + \alpha$.

PROPOSITION A.1. *Given any two sets X, \tilde{X} of n points as defined above such that $|x_i - \tilde{x}_i| \leq \alpha x_i \forall i$. For any $k \geq 1$, the difference between the optimal loss of clusterings over X and \tilde{X} are bounded as,*

$$|L(M^*) - L_q(\tilde{M}^*)| \leq \alpha \quad (2)$$

PROOF. We first show that $L_q(\tilde{M}^*) \leq L(M^*) + \alpha$.

$$\begin{aligned} L_q(\tilde{M}^*) &= \frac{1}{n} \sum_{i=1}^n |\tilde{\mu}_{\tilde{M}^*}(i) - \tilde{x}_i| \leq \frac{1}{n} \sum_{i=1}^n |\mu_{M^*}(i) - \tilde{x}_i| \\ &\leq \frac{1}{n} \left(\sum_{i=1}^n |\mu_{M^*}(i) - x_i| + \alpha \sum_{i=1}^n x_i \right) \leq L(M^*) + \alpha \end{aligned} \quad (3)$$

In Equation (3), the first inequality follows from the fact that \tilde{M}^* is the optimal clustering over \tilde{X} and hence replacing the cluster centers $\tilde{\mu}_{\tilde{M}^*}(i)$ with $\mu_{M^*}(i)$ leads to a quantity which is greater than equal to $L_q(\tilde{M}^*)$. The next inequality follows from triangle inequality and uses the fact that $|x_i - \tilde{x}_i| \leq \alpha x_i$. Using similar arguments, one can verify that $L(M^*) \leq L_q(\tilde{M}^*) + \alpha$. Combining the two equations, we have that $|L(M^*) - L_q(\tilde{M}^*)| \leq \alpha$ which is the main statement of the proposition.

The proof for $L(M^*) \leq L_q(\tilde{M}^*) + \alpha$ follows similar arguments leading to the main statement of the result. \square

REMARK A.1. *The results show that the difference between optimal loss of k -means clustering over inputs X and its grouped counterpart \tilde{X} is bounded by α . Building upon this, we will show that when the*

clustering is performed with sample-weighted k -means++, the expected loss over \tilde{X} is bounded by the optimal loss over X and α^2 .

To keep notations close to [6], we denote the loss over squared norm as $\phi(M) = \frac{1}{n} \sum_{x \in X} \min_{\mu \in M} |x - \mu|^2$. The loss $\phi_q(M)$ is defined similarly over \tilde{X} : $\phi_q(\tilde{M}) = \frac{1}{n} \sum_{\tilde{x} \in \tilde{X}} \min_{\tilde{\mu} \in \tilde{M}} |\tilde{x} - \tilde{\mu}|^2$.

PROPOSITION A.2. *Given any two sets X, \tilde{X} of n points as defined above such that $|x_i - \tilde{x}_i| \leq \alpha x_i \forall i$. For any $k \geq 1$, let \hat{M} be the clustering obtained by applying weighted k means++ (Algorithms 3 and 1) over the set \tilde{X} . Then,*

$$E[\phi_q(\hat{M})] \leq 16(\ln k + 2)(\phi(M^*) + \alpha^2) \quad (4)$$

PROOF. We first upper bound the optimal loss $\phi_q(\tilde{M}^*)$ with $\phi(M^*)$ and α . See that

$$\begin{aligned} \phi_q(\tilde{M}^*) &= \frac{1}{n} \sum_{i=1}^n |\tilde{\mu}_{\tilde{M}^*}(i) - \tilde{x}_i|^2 \leq \frac{1}{n} \sum_{i=1}^n |\mu_{M^*}(i) - \tilde{x}_i|^2 \\ &\leq 2 \left(\frac{1}{n} \sum_{i=1}^n |\mu_{M^*}(i) - x_i|^2 + \frac{\alpha^2}{n} \sum_{i=1}^n x_i^2 \right) \leq 2(\phi(M^*) + \alpha^2) \end{aligned} \quad (5)$$

Applying weighted- k means++ (Algorithms 3 and 1) over the set \tilde{X} produces \hat{M} . Using Theorem 1.1 in [6], we have that $E[\phi_q(\hat{M})] \leq 8(\ln k + 2)(\phi_q(\tilde{M}^*))$ and using Eq. 5 to replace $\phi_q(\tilde{M}^*)$, we obtain the main statement of the proposition. \square

REMARK A.2. *The result implies that Algorithms 1 and 3 is $O(\ln k)$ -competitive with $\phi(M^*) + \alpha^2$ while being orders of magnitude faster in comparison with the vanilla k -means++ which is $O(\ln k)$ -competitive with $\phi(M^*)$.*

We now analyze certain conditions where the clustering memberships of every point in the two cases (X and \tilde{X}) would be identical. Let $C = \{X_1, \dots, X_k\}$ be a clustering (or partition) of $X \subseteq [0, 1]$ with centers $M = \{\mu_1, \dots, \mu_k\}$. For all $x \in X_i$, and $i \neq j$, $|x - \mu_i| \leq |x - \mu_j|$. Let the minimum distance between any two points in two different clusters in C be the split of the clustering denoted as $\text{split}_C(X)$. Let the maximum distance between any two points in the same cluster be the width of the clustering denoted as $\text{width}_C(X)$.

DEFINITION A.1. [8] *A clustering $C = \{X_1, \dots, X_k\}$ of $X \subseteq [0, 1]$ is σ -separable for $\sigma \geq 1$ if $\text{split}_C(X) > \sigma \cdot \text{width}_C(X)$.*

In other words, any clustering C is σ -separable if the minimum distance between any two points in separate clusters is greater than the maximum distance between two points in the same cluster.

We now show that if the optimal clustering over the set X is σ -separable, then for small enough α depending on the value of σ , the optimal clustering over X and \tilde{X} will be the same. First note that, if a σ -separable clustering C exists for a given set of inputs, then only one such partitioning of the inputs.

LEMMA A.1. [5] *If there exists a k -clustering C of X , for $k \geq 2$, such that C is σ -separable, then there is only one such partitioning of X .*

The proof of the above Lemma can be found in [5]. We now show that if $\alpha < \frac{\text{split}_C(X) - \text{width}_C(X)}{4}$, then the same partitioning over \tilde{X} is also σ -separable and hence the optimal clustering for both X and \tilde{X} are identical.

Let s_1 and s_2 be the two points in X such that the distance between them is minimum among all pairs of points in separate clusters ($|s_2 - s_1| = \text{split}_C(X)$). Let w_1 and w_2 be two points in X such that the distance between them is maximum among all pairs of points in the same cluster.

For the points in X to have a σ -separable clustering in \tilde{X} , the following condition should hold in the worst case,

$$\begin{aligned} s_2(1 - \alpha) - s_1(1 + \alpha) &> w_2(1 + \alpha) - w_1(1 - \alpha) \\ \implies (s_2 - s_1) - \alpha(s_1 + s_2) &> (w_2 - w_1) + \alpha(w_1 + w_2) \end{aligned}$$

$$\implies \alpha < \frac{(s_2 - s_1) - (w_2 - w_1)}{4} = \frac{\text{split}_C(X) - \text{width}_C(X)}{4}$$

This implies that if the original clusters are σ -separable and α is small enough then the optimal cluster memberships over X and \tilde{X} will be identical.

A.2.2 Weighted K-Means++ Initialization. Initialization of the cluster centroids influences the quality of the resulting clusters formed by K-means [33]. We extend the K-means++ [6] algorithm for initialization with support for sample weights, 3 provides a sketch of this process.

Algorithm 3: Weighted K-Means++ Initialization

Require: X {Input data points}
Require: W {Input sample weights}
Require: k {Number of clusters}

- 1: $C \leftarrow X[\text{random_choice}(W)]$ {Initialize the first centroid randomly according to weights}
- 2: **for** i in 2 to k **do**
- 3: $D \leftarrow \text{min_distance}(X, C)$ {Compute distance of each point to nearest centroid}
- 4: $D \leftarrow D \cdot W$ {Weight the distances}
- 5: $P \leftarrow D / \text{sum}(D)$ {Compute probabilities}
- 6: $C \leftarrow C \cup X[\text{random_choice}(P)]$ {Select new centroid}
- 7: **end for**
- 8: **return** C

A.3 QUANTIZATION CONFIGURATION MANAGER

A.3.1 Configuration Search Space. This section outlines the range of values used for the configuration parameters for all the compression systems evaluated in this paper. More specifically, Tables 7 to 10 contain parameter values of config cubes for DynaQuant, QD+, CNR+, and GOBO+ respectively.

A.3.2 Additional Details for Guided Exhaustive Search. To avoid additional computation workload due to an exhaustive search through the vast configuration search space of DynaQuant, we designed a guided exhaustive search mechanism to speed up computation. Algorithm 4 describes the details of the proposed guided exhaustive search.

Parameter	Values
Number of bins	4, 6, 8, 12, 16, 32
Number of bins (Embedding Layers)	16, 32
Pruning Fraction	0, 0.1, 0.2, 0.3, 0.4, 0.5
Pruning Metric	Magnitude, Sensitivity
Protection Fraction	0.0005, 0.005, 0.01

Table 7: Search space for DynaQuant quantization configuration

Parameter	Values
Minimum number of bins	8, 16, 32, 64, 128, 256
Maximum number of bins	8, 16, 32, 64, 128, 256

Table 8: Search space for QD+ quantization configuration

Parameter	Values
Number of bins	8, 16, 32, 64, 128, 256
Number of step bins	10, 25, 50, 100
Range	0.1, 0.2, 0.3, 0.4, 0.5

Table 9: Search space for CNR+ quantization configuration

Parameter	Values
Number of bins	8, 16, 32, 64, 128, 256
Number of bins (Embedding Layers)	16, 32
Outlier threshold	-4
Max Iteration	1000

Table 10: Search space for GOBO+ quantization configuration

B DELTA ENCODER

B.1 Additional Details for Parameter Rearrangement

Section 6.3 details how parameter rearrangement alleviates poor run-length encoding compression. Algorithms 5 and 6 provide a sketch of the proposed rearrangement scheme and subsequent construction of the original checkpoint.

C EVALUATION SETUP

C.1 Datasets Used for Evaluation

Table 11 describes the vast array of ML tasks and datasets used for the experimental evaluation. These datasets have been used in the use cases of pre-training and transfer learning. By running experiments on both image and text datasets, we demonstrate the generalizability of DynaQuant on both modalities. Moreover, the wide array of tasks illustrates DynaQuant’s applicability for prevalent Machine Learning use cases.

C.2 Model Implementations

For pre-training the ResNet-152 and ViT-32L models on Imagenet1k, we utilize the implementation and hyperparameters available in the Torchvision package [63], while BERT-Base and GPT-2 Medium training leverages implementations provided by MosaicML [4] and NanoGPT [56] repositories respectively. Notably, we maintain the original training duration and model

Algorithm 4: Guided Exhaustive Search

Require: Quality threshold T , Configuration cube C_{cube} , Compression Ratio CR_{max}
Ensure: Optimal configuration C_{opt}

- 1: $C_{\text{opt}} \leftarrow \text{Null}$
- 2: $CR_{\text{max}} \leftarrow 0$
- 3: $\text{Diagonal} \leftarrow \text{GetDiagonal}(C_{\text{cube}})$
- 4: $C_{\text{opt}}, CR_{\text{max}} \leftarrow \text{ParallelSearch}(\text{Diagonal}, T)$
- 5: $\text{SubCubes} \leftarrow \text{GetFeasibleSubCubes}(C_{\text{cube}}, C_{\text{opt}})$
- 6: **for** each SubCube in SubCubes **do**
- 7: $C_{\text{temp}}, CR_{\text{temp}} \leftarrow \text{GuidedExhaustiveSearch}(T, \text{SubCube})$
- 8: **if** $CR_{\text{temp}} > CR_{\text{max}}$ **then**
- 9: $C_{\text{opt}} \leftarrow C_{\text{temp}}$
- 10: $CR_{\text{max}} \leftarrow CR_{\text{temp}}$
- 11: **end if**
- 12: **end for**
- 13: **return** C_{opt}

Algorithm 5: Rearranging parameters for efficient encoding

Require: Δ (Delta values calculated from adjacent checkpoints)
Require: C_q^{i-1} (The quantized integer values of the last checkpoint)
Ensure: Delta groups (A dictionary containing delta values for each unique quantization bin)

- 1: $\text{bins} \leftarrow \text{unique_bins}(C_q^{i-1})$
- 2: $\text{delta_groups} \leftarrow \text{create_empty_dict}(\text{bins})$
- 3: **for** $j \in [0, \text{length}(C_q^{i-1})]$ **do**
- 4: $\text{delta_groups}[C_q^{i-1}[j]].\text{append}(\Delta[j])$
- 5: **end for**
- 6: **return** delta_groups

Algorithm 6: Reconstructing parameters after rearrangement

Require: delta_groups (Delta groups obtained from the rearranging step)
Require: C_q^{i-1} (The quantized integer values of the previous checkpoint)
Ensure: C_q^i (The quantized integer values of the current checkpoint)

- 1: $C_q^i \leftarrow \text{create_zero_array}(\text{length}(C_q^{i-1}))$
- 2: **for** $j \in [0, \text{length}(C_q^{i-1})]$ **do**
- 3: $\text{bin} \leftarrow C_q^{i-1}[j]$
- 4: **if** $\text{delta_groups}[\text{bin}] \neq \emptyset$ **then**
- 5: $C_q^i[j] \leftarrow C_q^{i-1}[j] + \text{delta_groups}[\text{bin}].\text{pop}(0)$
- 6: **end if**
- 7: **end for**
- 8: **return** C_q^i

Dataset	Task	Training Mode
Imagenet [20]	Image Classification	Pre-training
C4 [74]	Masked Language modeling	Pre-training
Openwebtext [35]	Next Token Prediction	Pre-training
GLUE STS-B [83]	Semantic Textual Similarity	Transfer Learning
GLUE MNLI [83]	Natural Language Inference	Transfer Learning
Alpaca [81]	Instruction Fine-Tuning	Transfer Learning

Table 11: Summary of datasets used for evaluation

hyperparameters, avoiding any potential skewing of evaluation results, with the exception of GPT-2 Medium where we truncate

the training procedure to 30 billion tokens to restrict the training duration. In ViT-32L we find that the default parameters result in unstable training, so we reduce the learning from 0.003 to 0.001.

D RELATED WORK

D.1 Model Compression

Model compression techniques aim to reduce the storage, memory, and computational requirements of deep learning models without significantly compromising their performance (i.e. accuracy, perplexity, etc.). In this subsection, we discuss quantization and pruning, two popular architecture-preserving model compression approaches that allow for reduced storage size of the model weights.

Quantization. Quantization has been widely studied in the literature, especially in the context of model inference which benefits from the smaller memory footprints and faster computation.

In order to quantize models for efficient inference, Post-Training Quantization (PTQ) techniques [7, 11, 16, 31, 45] are commonly utilized where the model quantization is applied after the model is fully trained. On the other hand, Quantization-Aware Training (QAT) methods [17, 38, 48, 61, 76, 80] augment the training process to incorporate quantization errors into the loss function. QAT and *in-training* checkpoint quantization that we present in this paper differ in that the latter does not affect the training optimization function to aid quantization, but rather performs quantization on the intermediate model states during training.

Variable bit-width quantization assigns different bit-widths to model layers based on their importance, determined by metrics such as gradient magnitudes, Fisher information, or Hessian eigenvalues [14, 23, 24, 29, 53, 60]. This approach enables better compression without compromising performance. However, determining the optimal bit-width for each layer is difficult and time-consuming, often requiring additional fine-tuning. In DynaQuant, we present a novel non-uniform quantization approach based on approximate k-means clustering that enables high-quality quantization with minimal computational overhead.

Pruning. Pruning is another popular model compression technique in which unimportant parameters are removed from the model. Popular strategies to determine parameter importance include magnitude-based and sensitivity-based schemes.

Magnitude-based pruning techniques remove parameters with the smallest absolute values, assuming that they contribute less to the model’s output [41]. While, sensitivity-based pruning methods consider the impact of parameter removal on the model’s performance or loss, by considering the Taylor series approximation of loss change [19, 28, 82, 90].

Prior work considered either magnitude or sensitivity-based pruning. We argue that neither is sufficient and a combination of both is required. Shen et al. [77] show that magnitude-based pruning can suffer from poor performance during the early phase of training. The computation of the sensitivity metric is performed by factoring in the magnitude of parameter gradients during training, this approach can be ineffective when the model has already been trained to convergence, i.e. the gradients are close to

zero. To avoid this problem, some post-training pruning systems [43, 58] adopt second-order Taylor series approximations that use the Hessian trace or eigenvalues. While robust, these methods have high computational costs. In this paper, we adopt a novel parameter ranking scheme that combines both magnitude and first-order sensitivity metrics to minimize the compression overhead while preserving the quality.

Furthermore, prior work on model pruning has been primarily focused on either pruning before the training begins or after the completion of the training process. In this paper, we consider *in-training* pruning, that is, the intermediate model state during training. The recent work on Lottery Ticket Hypothesis with Rewinding [32] has shown that simple magnitude-based heuristics can be used to identify extremely sparse subnetworks early in training that yield performance similar to the full network when trained in isolation. We leverage this insight and show that for some models up to 40% of model parameters can be pruned during checkpointing with negligible loss in quality.

D.2 Checkpointing at Scale

As machine learning models become increasingly large and complex, distributed checkpointing has emerged as a necessity. Distributed checkpointing systems [27, 69] save partial model

states across multiple nodes within a distributed system, instead of relying on a single process to store the entire model state. This approach proves especially useful when the model state cannot fit on a single device. Additionally, distributed checkpointing reduces the overhead associated with the storage and retrieval of large checkpoints. Our proposed method is fully compatible with distributed checkpointing, enabling checkpoint compression even when the model state is distributed across different processes. Frequent checkpointing is another crucial aspect of model checkpointing systems. By creating checkpoints more frequently, the risk of losing progress due to unexpected failures is minimized, allowing for more granular control over the training process. CheckFreq [66] facilitates frequent checkpointing through a novel two-phase process that overlaps computation with the checkpointing operation. It also dynamically determines checkpointing intervals to balance the trade-offs between overhead and wasted work. However, to limit storage requirements, CheckFreq retains only the two most recent checkpoints, which restricts the system’s flexibility to resume training at different points in time. A combination of such frequent checkpointing systems along with a delta compression system can minimize the storage overhead while still providing a lot of flexibility to the user.